Click Here for Full Article

Dynamic control on serpentine crystallization in veins: Constraints on hydration processes in oceanic peridotites

M. Andreani
Géosciences Marines, CNRS, IPGP, 4 Place Jussieu, F-75252 Paris Cedex 5, France

Now at Laboratoire de Tectonophysique, Université Montpellier 2, Place Eugène Bataillon, Case 49, F-34095 Montpellier, France (andreani@msem.univ-montp2.fr)

C. Mével
Géosciences Marines, CNRS, IPGP, 4 Place Jussieu, F-75252 Paris Cedex 5, France

A.-M. Boullier
LGIT, CNRS, BP 53, F-38041 Grenoble Cedex 9, France

J. Escartín
Géosciences Marines, CNRS, IPGP, 4 Place Jussieu, F-75252 Paris Cedex 5, France

[1] Deformation and hydration processes are intimately linked in the oceanic lithosphere, but the feedbacks between them are still poorly understood, especially in ultramafic rocks where serpentinization results in a decrease of rock density that implies a volume increase and/or mass transfer. Serpentinization is accompanied by abundant veining marked by different generations of vein-filling serpentines with a high variety of morphologies and textures that correspond to different mechanisms and conditions of formation. We use these veins to constrain the role of deformation and mass transfer processes during hydration of oceanic peridotites at slow-spreading ridges. We have selected a representative set of veins from ocean floor serpentinites of the Mid-Atlantic Ridge near Kane transform fault (23°N) and characterized these in detail for their microstructures and chemistry by coupling optical and electron microscopy (SEM, TEM) with electron microprobe analyses. Four main veining episodes (V1 to V4) accompany the serpentinization. The first episode, identified as vein generation V1, is interpreted as the tectonically controlled penetration of early seawater-dominated fluid within peridotites, enhancing thermal cracking and mesh texture initiation at 3–4 km up to 8 km depth and at T <300–350°C. The two following vein stages (V2 and V3) formed in a closed, diffusive system and accommodate volume expansion required to reach almost 50% serpentinization of the protolith. The cracks exploited by these veins were caused by the progressive unroofing at depths of ∼4 to ∼2 km along a detachment fault. Degree and rate of serpentinization seem to be controlled by the capacity of the system to create space and to drive the mass transfer needed for ongoing serpentinization, and this capacity is in turn linked to the exhumation rate and local tectonics. During this period, water consumed by hydration may prevent the establishment of convective hydrothermal cells. The onset of an open hydrothermal system in the shallow lithosphere (<2 km), where brittle fracturing and advective transfer dominate and enable the completion of serpentinization, is marked by the last vein generation (V4). These results show a complete history of alteration, with the crystallization of different types of serpentine recording different tectonic events, chemical conditions, and modes of hydrothermal alteration of the lithosphere.

1. Introduction

[2] Exposures of serpentinized ultramafic rocks are common along slow- and ultra-slow spreading ridges, and preferentially at the end of segments [*Cannat et al.*, 1995a; *Dick*, 1989; *Lagabrielle et al.*, 1998]. These outcrops correspond to deep lithospheric materials exhumed during episodes of low magmatic supply along large-offsets faults (detachments) and testify to a compositionally heterogeneous lithosphere that includes mantle and magmatic rocks [*Cannat*, 1993; *Cann et al.*, 1997; *Karson and Lawrence*, 1997]. Serpentinization of ultramafic rocks considerably modifies, among other things, the rheological [e.g., *Moore et al.*, 1997; *Escartín et al.*, 1997, 2001], petrophysical [e.g., *Christensen*, 1972; *Brown and Karson*, 1988; *Carlson and Miller*, 1997; *Dyment et al.*, 1997; *Miller and Christensen*, 1997] and chemical [e.g., *Janecky and Seyfried*, 1986] properties of the oceanic lithosphere. Serpentinization has been identified as a source of hydrogen and hydrocarbon-rich fluids that can sustain very primitive microbial activity at hydrothermal vents [*Janecky and Seyfried*, 1986; *Charlou et al.*, 1998; *Holm and Charlou*, 2001; *Kelley et al.*, 2001]. Heat released during serpentinization may be able to drive hydrothermal circulation [*Lowell and Rona*, 2002; *Emmanuel and Berkowitz*, 2006], but this aspect is still controversial [*Allen and Seyfried*, 2004]. Geological and geophysical observations demonstrate that an important degree of alteration is acquired at the ridge axis, and the gradual increase of seismic velocities to mantle velocities was interpreted as a decrease in serpentinization with depth [e.g., *Canales et al.*, 2000].

[3] The maximum depth and mechanisms of fluid penetration and circulation in the oceanic lithosphere are still poorly constrained, partly because of the complex feedback between the processes involved, including tectonic unroofing, hydration reactions, and fluid hydrodynamics, and because of the difficulty of interpreting geophysical images in terms of lithology. Geological constraints on the initiation and evolution of the serpentinization process through time at the ridge axis are thus needed to understand this complex alteration, its role in tectonic and hydrothermal processes at mid-ocean ridges and, eventually, during subduction of oceanic lithosphere.

[4] Lithosphere hydration is associated with the formation of metamorphic veins that are records of fluid/rock interaction, mass transfer and deformation history. Serpentine veins in hydrated peridotites are particularly abundant and display a vast and complex variety of textures and morphologies [e.g., *Dilek et al.*, 1997]. This variety reflects numerous mechanisms of vein formation recorded by different serpentine mineral assemblages and fluid conditions.

[5] Serpentines are tri-octahedral sheet silicates ($Mg_3Si_2O_5[OH]_4$) that include four main structural types: lizardite (planar structure), chrysotile (cylindrical structure), polygonal serpentine (tubular with a polygonized section) and antigorite (modulated structure) (cf. review by *Wicks and O'Hanley* [1988]). These various microstructures reflect different wrapping modes of tetrahedral (T) and octahedral (O) sheets in response to their geometrical misfit, as the lateral dimension of O layers is 3 to 5% greater than that of T layers [*Wicks and Whittaker*, 1975]. Al and Fe^{3+} substitutions may substitute Si in tetrahedral sites, while the Mg in octahedral sites can be substituted primarily by Fe^{2+}, Fe^{3+}, Al, and, to a lesser extent, by Cr, Ni and Mn. Under serpentinization conditions of oceanic peridotites (T < 450–500°C [*Früh-Green et al.*, 1996; *Agrinier and Cannat*, 1997; *Grobety et al.*, 1997]), all serpentines can be found owing to their stability over a wide temperature domain
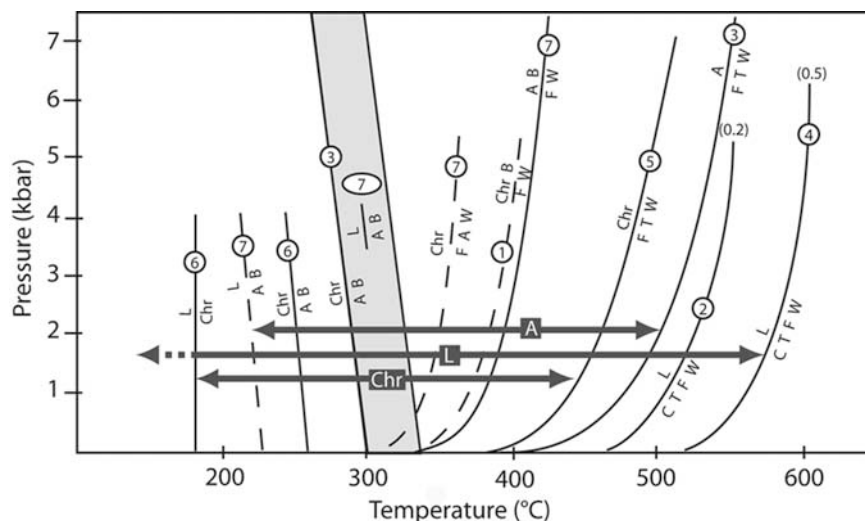
Figure 1. Phase diagram in the MSH system for the 3 main structural types of serpentine realized with compiled available data from experimental, theoretical, and natural studies of (1) *Johannes* [1968], (2) *Chernosky* [1973], (3) *Evans et al.* [1976], (4) *Caruso and Chernosky* [1979], (5) *Chernosky et al.* [1988], (6) *O'Hanley and Wicks* [1995], and (7) *Evans* [2004]. Complementary curves from the MASH system are added to represent the enlarged stability field of lizardite as a function of its Al content, given in xAl by the number in brackets (xAl = 0,2 is equivalent to $Al_2O_3 = 3.7$ wt%, and xAl = 0,5 is equivalent to $Al_2O_3 = 9.2$ wt%). A, antigorite; B, brucite; C, chlorite; Chr, chrysotile; L, lizardite; F, forsterite; T, talc; W, H_2O.

(<600°C) with negligible P dependence (Figure 1 and references therein). Recent experimental studies in static hydrothermal systems [*Grauby et al.*, 1998; *Normand et al.*, 2002] show that the occurrence of different serpentine types (primarily chrysotile and lizardite) are dominantly controlled by the reaction kinetics (Figure 2) rather than by P or T conditions [*Evans*, 2004]. In natural settings, deformation processes can also modify physicochemical conditions and therefore affect serpentine crystallization [*Andreani et al.*, 2004]. Serpentine vein microstructures are thus potential tools to identify and constrain different deformation and fluid-rock processes, and their interactions in oceanic peridotites.

[6] Here we present a detailed study of the different serpentine veins sampled outside mafic/ultra-mafic contact zones in a representative suite of rocks drilled from ODP Holes 920B and 920D, at the flank of the Mid-Atlantic Ridge near its intersection with the Kane transform fault (MARK area, 23°N, ODP Leg 153). Characterization of the different serpentine vein types (texture, chemistry, micro- and nano-structure) were determined by coupling scanning electron microscopy (SEM), transmission electron microscopy (TEM) and electron probe micro-analyses (EPMA). The correlation between mineralogical, chemical and structural data enables an interpretation of serpentine crystallization microstructures in veins in terms of system dynamics (deformation mechanism, system openness, mass transfer process), and an interpretation of the temporal progression of vein microstructure in relation to the overall alteration state of the upper lithosphere. These results are coupled

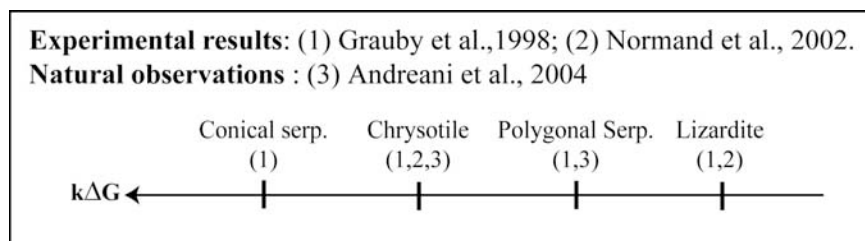**Figure 2.** Role of kinetic effects on microstructure crystallization in serpentine synthesis [*Grauby et al.*, 1998] and olivine dissolution [*Normand et al.*, 2002] experiments compared to available natural observations [*Andreani et al.*, 2004].

with available geophysical data to constrain the evolution of the serpentinization process at the MARK area in particular, and that of oceanic lithosphere formed along slow spreading ridges in general.

2. Geological Setting

[7] Serpentinized harzburgites crop out along the western fault scarp bounding the Mid-Atlantic Ridge valley at 23°21N, and 30 km south of its intersection with the Kane transform fault (MARK area, Figure 3). The peridotite outcrops, first identified from submersible studies and sampled through dredging [Karson et al., 1987; Mével et al., 1991], extend as a belt parallel to the axis and appear to be associated with a magnetic anomaly that may result from the high magnetic susceptibility of serpentinites [Brown and Karson, 1988]. Seismic refraction profiles across the area show a complex velocity structure that indicates that the thickness and nature of the crust varies laterally. Interpretation of the seismic velocity structure at ODP Site 920 shows a continuous velocity gradient that increases to reach mantle velocities (~8 km/s) at ~3–4 km below seafloor (Figure 4), suggesting a decrease in serpentinization with depth below the ODP site. The axial structure, in contrast, shows a thick (>5 km) crust with the possible presence of melt in the lower crust only ~6 km east of the drill site [Canales et al., 2000]. The seismic Moho in this area, defined by the ~7.2–7.5 iso-velocity contour, shows variations in depth of up to 2–3 km over distances of <10 km. This area, which is spreading at a full-spreading rate of ~2.7 cm/year, underwent an eastward ridge jump ~0.7 to 1 m.y. ago. The major rift-bounding faults are relatively steep (40–70°) and intersect an earlier, more pervasive, east- and shallowly dipping (20–40°) fabric well identified from submersible dives [Karson et al., 1987; Mével et al., 1991]. Sheared serpentinites, gabbros and rocks with high-temperature plastic fabrics were collected along this continuous fault scarp, whose dip decreases away from the axis. The shallowly dipping structures present the characteristics of an oceanic detachment fault plane similar to those observed in other MAR areas [e.g., Cann et al., 1997; Tucholke et al., 1998]. They are interpreted as related to earlier low-angle normal faults and shear zones that accommodated the tectonic extension of the axial lithosphere and the exhumation of ultramafic rocks during a period of limited magmatic supply [Karson and Lawrence, 1997]. Local basaltic cap rocks overlie the serpen-

tinites and indicate limited, intermittent and very local volcanic eruptions.

[8] Serpentinite exposures were drilled on the footwall of the major detachment fault during ODP Leg 153 at Site 920, Holes B and D, located on the western flank of the median valley in oceanic crust <1 m.y. old (Figure 3). Oxygen and hydrogen isotopic studies of these rocks reveal that serpentinization at this site results essentially from interaction of seawater with peridotites at temperatures ranging from >350–400°C to 200°C [Hebert et al., 1990; Agrinier and Cannat, 1997]. Sulfur mineralogy, content, and isotopes suggest that seawater most probably reacted with mafic units before peridotite hydration at a maximum temperature of 400°C [Alt and Shanks, 2003].

3. Characteristics of MARK Serpentinites

[9] ODP Holes 920 B and D drilled ~126 m and ~200 m deep, respectively, with an overall recovery of 47%. Images of representative samples and textures from these holes are shown in Figure 5. The predominant rock type recovered is serpentinized harzburgite with the following average mode: 82% olivine, 15% orthopyroxene, 2% clinopyroxene and 1% of spinel [Cannat et al., 1995b]. The harzburgite shows a high-temperature plastic foliation, defined by oriented olivine and elongated pyroxene grains (Figures 5a and 5b), that dips at 30° on average [Ceuleneer and Cannat, 1997]. No other major deformation events have affected these massive samples, which preserve the different alteration stages marked by several veining episodes [Dilek et al., 1997]. Serpentinization degree along both holes varies between 50% and 100% as estimated by the Leg 153 shipboard scientific party from relic mineral abundances. Neither periodicity nor gradient of serpentinization is observed along the alteration profiles in these holes [Cannat et al., 1995b]. Rare pyroxene-rich horizons show minimum alteration degrees (down to 20%), but highly serpentinized peridotites (80% or higher) are the most abundant. The whole-rock serpentinization is homogeneous on a hole scale and associated with an anastomosing fabric of white fibrous serpentine veins and oxide alignments (Figure 5a) that is characteristic of the drilling sites. This fabric does not systematically follow the initial olivine crystal plastic foliation but is sub-parallel to the well-developed and shallowly dipping fabric observed during submersible dives. On a core scale, (one core is 1.5 meters) the
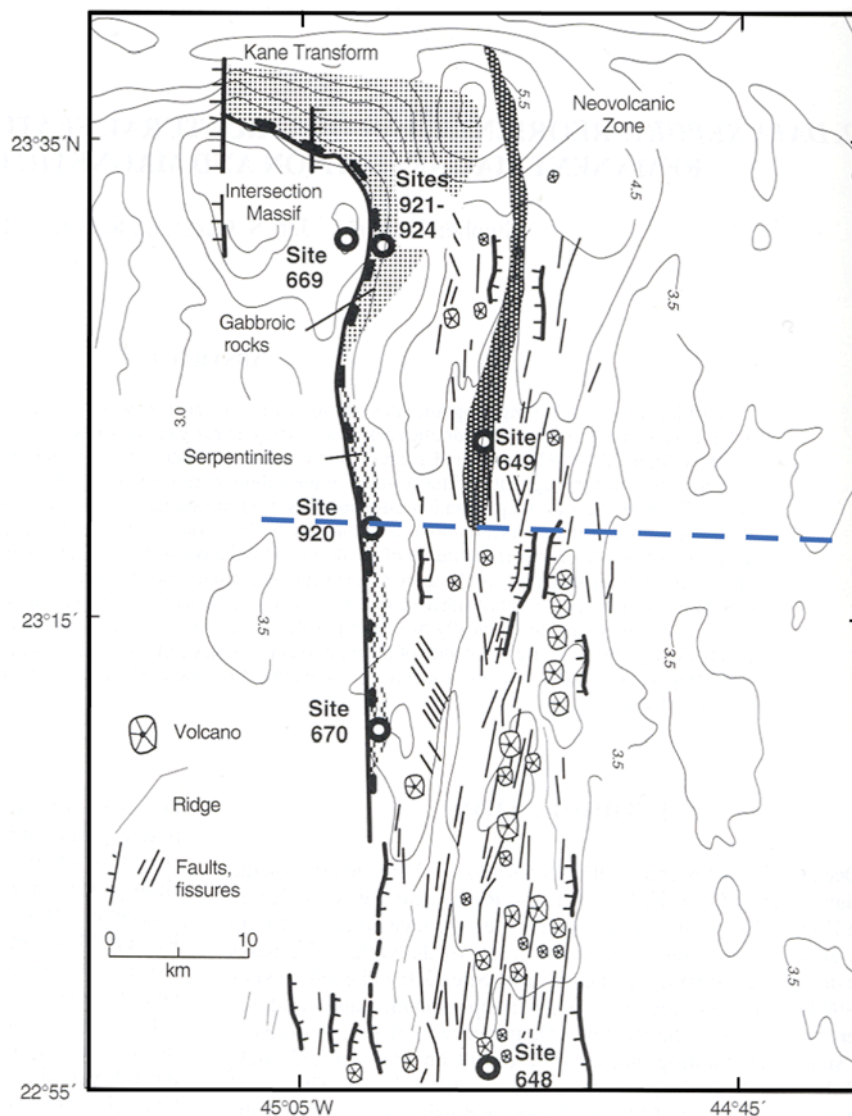
Figure 3. Tectonic map of the Mid-Atlantic Ridge near its intersection with the Kane transform fault (MARK area) with the location of serpentinite (wavy symbol), gabbros (light shaded), and basalt (dark shaded) outcrops identified from submersible studies and dredging. Serpentinites exposures extend as a belt under the detachment fault scarp which forms the western flank of the Mid-Atlantic Ridge valley. ODP drilling sites are shown as open circles. Contours are in km below sea level [*Cannat et al.*, 1995b]. The dashed blue line locates the seismic profile of Figure 4.

alteration can vary between two main textures: (1) a homogeneous serpentinization characterized by distributed fibrous veins and oxide alignments on a sample scale (Figures 5a, 5b, and 5c) and (2) an alternation of 1- to 2-cm-thick, fully serpentinized bands rich in fibrous veins and oxide alignments with partly serpentinized harzburgite bands without veins (Figure 5d). The widespread development of the pseudomorphic mesh and bastite texture after olivine and pyroxenes, respectively [*Wicks and Whittaker*, 1977; *Dungan*, 1979] in the whole rock indicates a pervasive background alteration. In addition to the serpentine veins, we find rare early magmatic veins, late carbonate veins, and very scarce chlorite veins. These veins are not related to the main hydration event of the lithosphere and are not included in this study.

4. Materials and Methods

[10] All core materials available from Holes 920B and 920D were examined macroscopically at the ODP repository in Bremen, Germany. A systematic and extensive re-sampling for this project was carried out to encompass representative samples containing the main serpentine vein types and
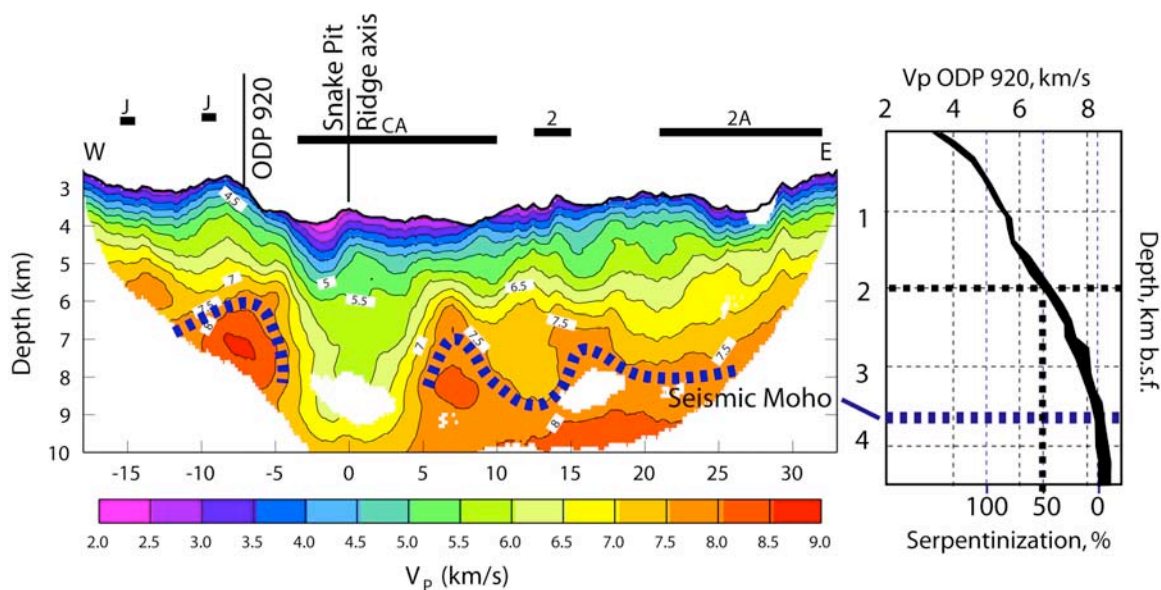
Figure 4. Seismic refraction profile across the Mid-Atlantic Ridge at site 920 and its interpretation (modified from *Canales et al.* [2000]). The Moho, defined by the velocity structure (mantle velocity ∼8 km/s), is depicted by the blue dotted line. It shows variations in depth of up to 2−3 km, over distances of <10 km in this area. The progressive increase of P wave velocity with depth is interpreted as a gradient of serpentinization.

alteration textures throughout the core. Twenty-five selected samples were used for petrographic examination, and electron microprobe analyses were done on nine selected thin sections. The complete list of selected samples and their core depth is given in Table 1. The small grain size of serpentine minerals (often <1 μm) is below the resolution of the optical microscopy, and therefore scanning (SEM) and transmission (TEM) electronic microscope observations are required to characterize the minerals and their crystallographic organization within vein infill. One TEM grid was prepared for each vein type, and the corresponding broken sample was observed and microstructurally analyzed under SEM.

[11] SEM images were performed on a JEOL 6320FEG scanning electron microscope at the CRMCN (Marseille, France) under a 15 kV accelerating voltage. Fragments of rocks containing veins were broken and prepared for SEM. After cleaning in an ultrasonic bath, they were glued on a sample holder and covered with a 10−15 nm thick carbon coating. TEM observations were performed on a JEOL 2000fx high-resolution transmission electron microscope under a 200 kV at the CRMCN (Marseille, France). Thin sections, glued with Crystal Bound® resin, were cut perpendicular to the veins. Single hole copper TEM grids were glued on selected areas of the section and extracted from the glass substrate by heating the resin. The

Table 1. Studied Samples From Sites 920B and 920D[a]

ODP Name	Depth of Top Interval, mbsf
Site 920B	
153_920B_1R2 pc1 13_17cm	1.2
153_920B_3R1 pc3 41_47cm	23.9
153_920B_3R1 pc5 87_92cm	24.3
153_920B_6R1 pc3 20_26cm	52.1
153_920B_6R1 pc8 75_81cm	52.6
153_920B_7R1 pc4 78_83cm	61.8
153_920B_7R2 pc8 113_117cm	63.5
153_920B_8R1 pc14 109_115cm	71.5
153_920B_12R2 pc6 147_150cm	110.5
153_920B_12R5 pc1 73_77cm	113.7
Site 920D	
153_920D_2R1 pc13 116_125cm	9.2
153_920D_4R2 pc8 66_71cm	31
153_920D_5R2 pc1 2_9cm	38
153_920D_10R2 pc7 116_120cm	80.5
153_920D_11R1 pc4 30_34cm	85.6
153_920D_11R3 pc7 89_93cm	88.8
153_920D_14R1 pc7 90_96cm	115.3
153_920D_14R2 pc4 30_34cm	116.1
153_920D_14R2 pc7 91_94cm	116.7
153_920D_16R1 pc1 10_14cm	143.5
153_920D_16R5 pc5 126_130cm	139.4
153_920D_16R6 pc10 66_69cm	140
153_920D_17R3 pc7 123_128cm	146.7
153_920D_19R1 pc7 61_65cm	162.8
153_920D_20R2 pc5 59_64cm	173.6

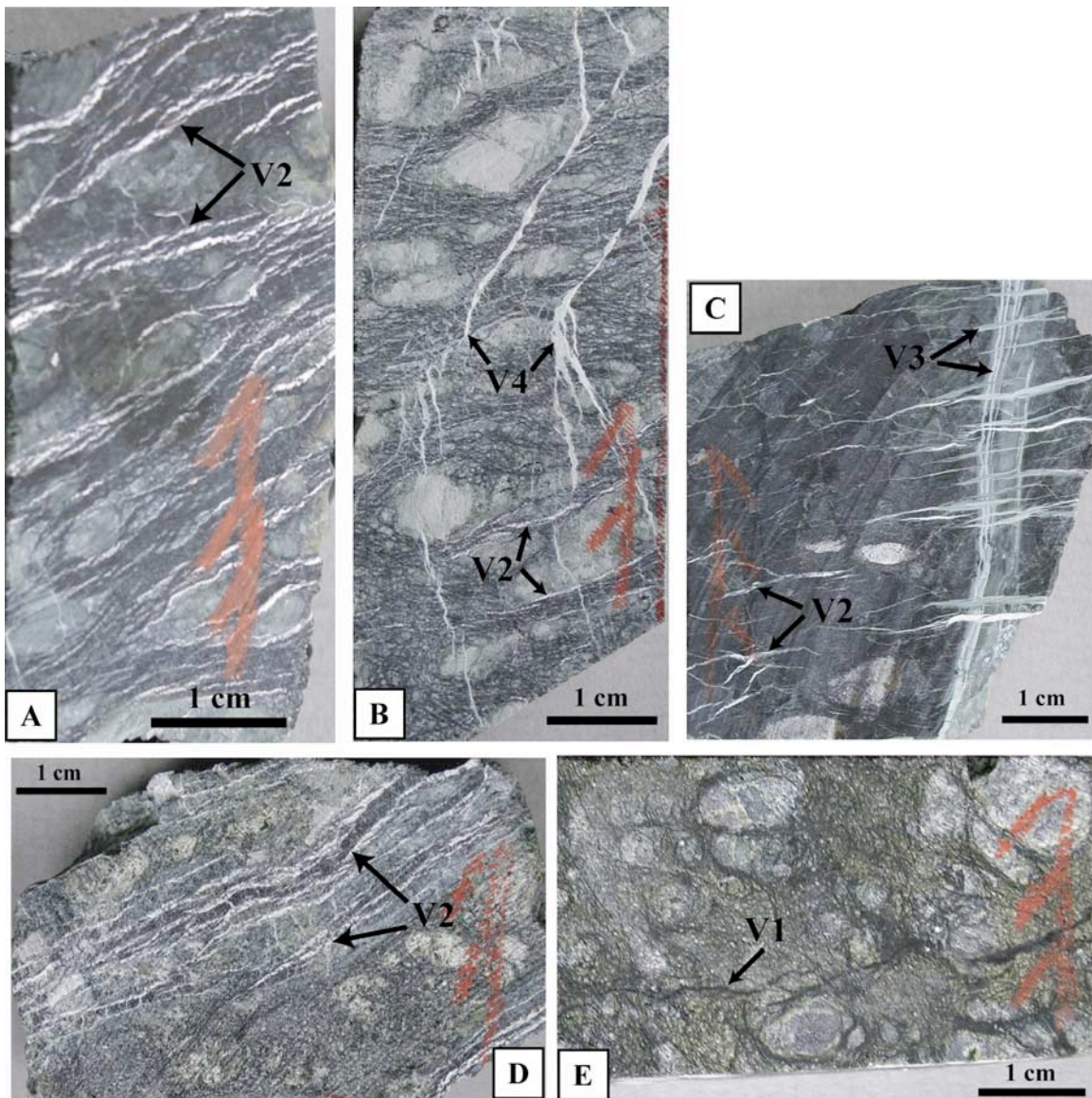[a] Top intervals depth is given in meters below seafloor (mbsf).

Figure 5. Representative samples of the serpentinized harzburgites collected during OPD leg 153 at site 920. (a) Sample 153-920B-3R-1, 41–47 cm; (b) Sample 153-920D-5R-2, 2–9 cm; (c) Sample 153-920D-19R-1, 61–65 cm; (d) Sample 153-920D-14R2, 30–34 cm; (e) Sample 153-920D-14R-2, 91–94 cm. The red arrow indicates the top of the section. Most of the samples are highly serpentinized (80–100%) with a few exceptions, such as that on Figure 5e or outside vein zones on Figure 5d (∼50% of alteration). The HT foliation is marked by elongated pyroxenes (Figures 5a and 5b). The different generations of veins identified correspond to the dark lines in Figure 5e (V1 veins), the most developed fibrous veins with an oblique fabric in Figures 5a, 5b, 5c, and 5d (V2 veins), the aqua-blue veins with different orientations on Figure 5c (V3 veins), and the latest white vein generation that cross cuts vertically the foliation in Figure 5b (V4 veins).

specimens were then thinned by ion-beam milling (Precision Ion Polishing System, Gatan 690) and carbon-coated.

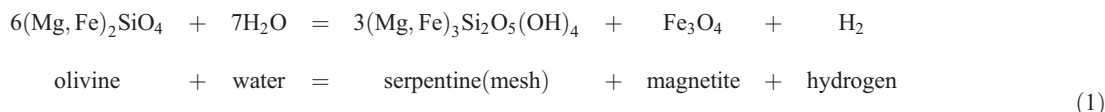[12] Micro-analyses of relict minerals, serpentine pseudomorphs, and serpentine veins were conducted on a Cameca SX50 electron microprobe at the Camparis service of the IPG-Paris (France). A 5 μm spot size was used in order to average the chemical composition of a texture on several serpentine grains, owing to the small grain size of many of the microtextures (see Section 5). Serpentine minerals occurring in different vein textures were measured for major elements (Mg,

Si, Al, Fe). In addition, the following minor elements were qualitatively measured: Cr, Ni, Ti, S, Cl, and F. Only Cr, Ni, and S were locally detected in significant amounts (above the detection limit) within these rocks. Compositions are reported in auxiliary material[1] Tables S1 through S3 and in oxide-weight percent (wt%) and in atom-per-formula unit (a.p.f.u.) calculated on the basis of seven anhydrous oxygens for serpentines.
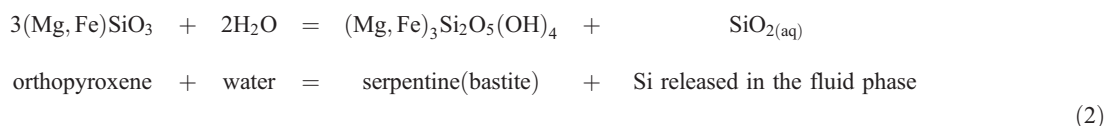
5. Serpentine Microtextures: Pseudomorphs and Veins

5.1. Mesh and Bastites Textures

[13] The main hydration textures are the classical pseudomorphic mesh and bastite textures replacing olivine and pyroxene, respectively, and represent the bulk of the lithosphere alteration in volume. These textures are characteristic of oceanic hydration under static conditions [e.g., *Wicks and Whittaker*, 1977; *Dungan*, 1979]. Mesh size varies between 0.3 to 1 mm. The mesh texture dominantly shows dark isotropic cores, sometimes with relict olivine, surrounded by a characteristic rim composed of lizardite and magnetite. No brucite $(Mg(OH)_2)$ was clearly identified in these rocks, thus the major serpentinization reaction of olivine (Fo80; Table S1) which produces serpentine and magnetite is

$$6(Mg,Fe)_2SiO_4 + 7H_2O = 3(Mg,Fe)_3Si_2O_5(OH)_4 + Fe_3O_4 + H_2$$

$$\text{olivine} + \text{water} = \text{serpentine(mesh)} + \text{magnetite} + \text{hydrogen}$$

(1)

[14] Hydration of pyroxene produces silica and should favor the formation of talc and/or tremolite [*Allen and Seyfried*, 2003]. However, pyroxenes in our samples (dominantly orthopyroxene) are replaced by serpentine, and clinopyroxenes are generally less altered. Talc and tremolite are seldom observed, suggesting that pyroxene probably alters in an Mg-dominated system controlled by olivine hydration. The exclusive formation of serpentine from orthopyroxene is

$$3(Mg,Fe)SiO_3 + 2H_2O = (Mg,Fe)_3Si_2O_5(OH)_4 + SiO_{2(aq)}$$

$$\text{orthopyroxene} + \text{water} = \text{serpentine(bastite)} + \text{Si released in the fluid phase}$$

(2)

[15] Even if magnetite, which forms within the mesh, is dominantly linked to olivine alteration,

_____
[1]Auxiliary materials are available at ftp://ftp.agu.org/apend/gc/2006gc001373.

magnetite can potentially be added to the previous reaction products in an amount inversely proportional to the ability of the serpentine minerals to incorporate iron in their structure during the different stages of hydration. These general serpentinization reactions will be discussed further in section 7.2. Cr-spinels (chromite) are variably altered to ferritchromite and, in a few cases, are surrounded by a chlorite aureole.

5.2. Veins

[16] In addition to the typical and well-studied mesh and bastite textures, we have identified four main types of serpentine veins based on textural and morphological criteria under an optical microscope with crossed polarized light. The relative age of these veining events (V1 through V4, V4 being the latest one) was deduced from cross-cutting relationships. The identification of serpentine types and their genetic relations in veins was accomplished by electron microscopy imaging.

5.2.1. V1 Vein Type

[17] V1 veins show an irregular shape, with their width varying from a few to several hundreds of micrometers (Figure 6). They are generally continuous at the sample scale (Figure 5e) and show no preferred orientation. While V1 veining occurs in almost all samples independent of the overall degree of serpentinization, we rarely observe more than one V1 vein per sample (i.e., on the order of ∼10 cm of core length). In the most altered samples, V1 veins are cross-cut by the other vein types, V2 through V4. Their main feature is a high magnetite concentration in clusters along the vein walls, enabling their identification in hand specimen. Magnetite is less abundant but present as isolated micrometric grains within the vein centers and the serpentine-alteration halo flanking the vein. The V1 infill is transparent under polarized light (Figure 6a) and generally shows an almost isotropic texture under crossed-polarized light
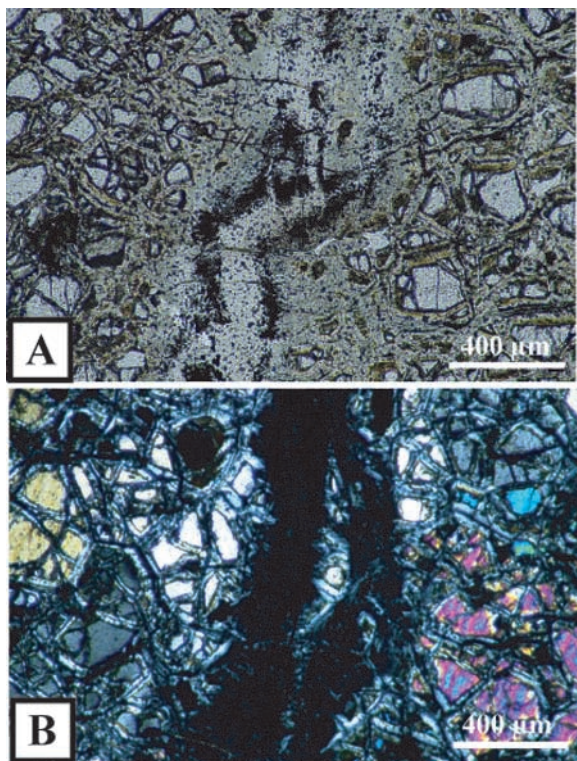
Figure 6. Serpentine vein of the V1 generation, marked by (a) oxide alignments on their walls when observed under polarized light and (b) a dark isotropic aspect under crossed-polarized light. They also present an alteration halo which is marked by the absence of relict olivine in close contact to the vein margins characterized by magnetite lineations.

(Figure 6b), with less isotropic segments showing micrometric circular extinction features. SEM images reveal that V1 veins are mainly filled by a homogenous, microgranular material in which spherical areas of several micrometers in diameter develop locally (Figure 7a). The homogeneous material is made of nanometric conical serpentine (conical chrysotile, tip of ~10 to 30 nm in diameter; Figures 7b and 8), with minor amounts of cylindrical serpentines (chrysotile, <100 nm in diameter; Figure 7b), that seems to grow from a poorly crystallized phase (protoserpentine). The spherical zones show a zoning from a poorly crystallized center to a progressive, radial growth of conical, cylindrical and then polygonal serpentine toward the exterior, at the expense of the homogeneous material outside. All these serpentine phases and their succession were reported in serpentine synthesis experiments as the first crystallization product evolving from magnesian gels [*Yada and Iishi*, 1974; *Devouard et al.*, 1997; *Grauby et al.*, 1998]. While chrysotile is common in natural rocks, protoserpentine has seldom been reported previously [*Viti and Mellini*, 1998; *Andreani et al.*, 2004], and the conical chrysotile is reported here for the first time in a natural setting.

5.2.2. V2 Vein Type

[18] V2 veins are lens-shaped and occur both as interconnected and isolated features. They can be up to several cm in length and a few mm in width (Figure 9). This second type of veins is by far the most widespread throughout the core. They form a major network responsible for the fabric visible at the outcrop scale and so characterize it (Figures 5a, 5b, 5c, and 5d). Their mean dip is ~35° but can locally be sub-vertical and is not necessarily parallel to the olivine-crystal plastic fabric. V2 veins are mainly observed within the olivine pseudomorphs where they tend to follow ancient olivine outlines (Figure 9b), their propagation being probably easier along the weak (001) planes of the lizardite mesh. They also cross-cut pyroxene crystals locally along their cleavage when properly oriented, or they bypass the pyroxenes, defining an undulating foliation when crystals are not properly oriented. Homogeneous parallel fibers link matching wall irregularities on both side of the veins and are an indicator of the opening vector (Figure 9b). Iron oxide alignments are generally observed along one of the vein walls, with elongated oxide grains parallel to the fibers locally incorporated within the vein.

[19] TEM observations confirm the homogeneous microtexture of these veins, whose infill is exclusively composed of long parallel nanotubes of chrysotile, with a diameter <50 nm, that are continuous and span the vein width. The nanotubes root all along the vein wall, following its contour and irregularities (Figure 10).

5.2.3. V3 Vein Type

[20] V3 veins are lens-shaped and not necessarily interconnected, in contrast with the second generation V2 veins. They can be distinguished from V2 in hand specimen as they are not fibrous and display an aqua-blue color (Figure 5c). Their length is highly variable; they can be only of a few mm long, or crosscut the core and have lengths of tens of cm. They are common throughout the cores (observed at least once in each 150 cm long core section), and, when observed along broken surfaces following individual veins, they show slicken-fibers recording a shear component of deformation during this veining event. They tend
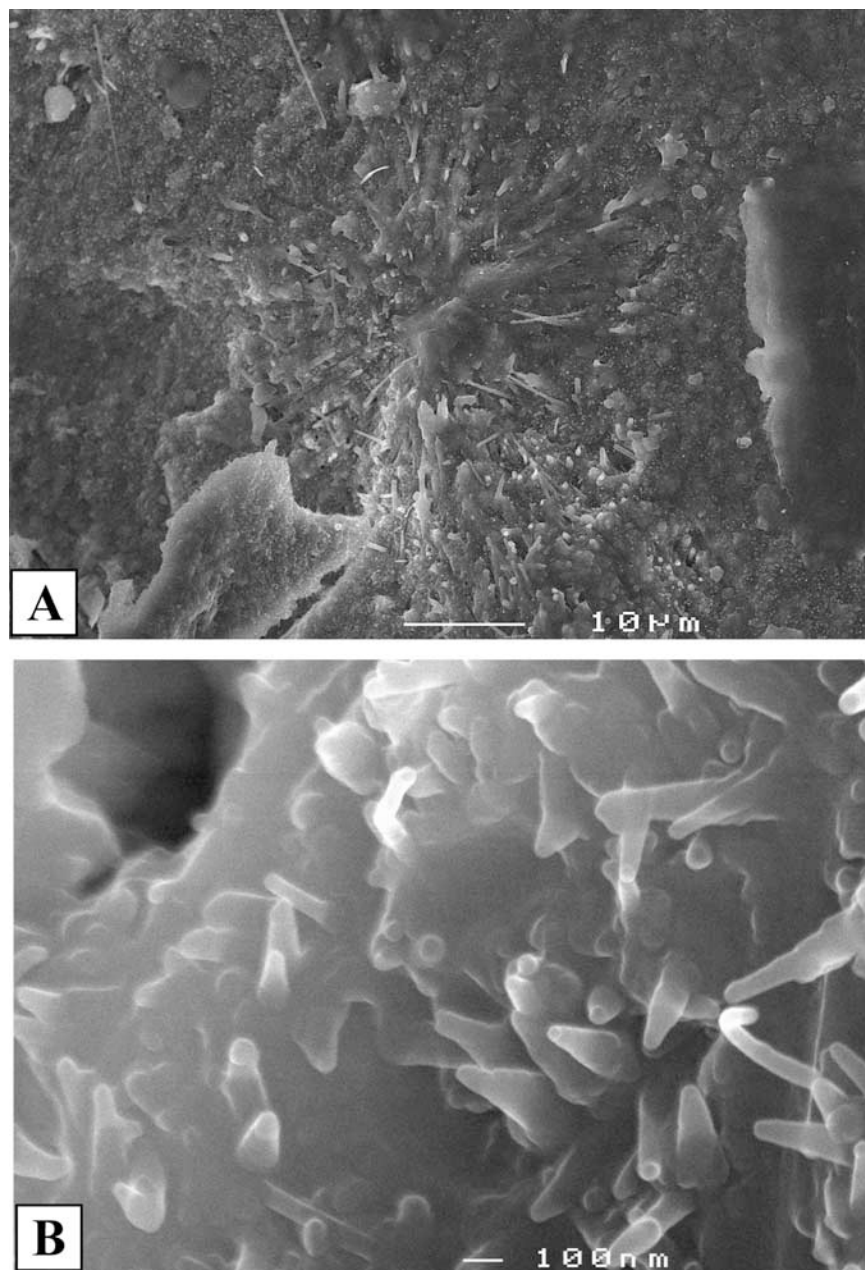
Figure 7. SEM images of the inner structure of V1 veins. (a) Radial crystallization features within a homogeneous microgranular material. (b) Conical chrysotile is the dominant serpentine type observed in these veins, associated with minor amounts of chrysotile (cylindrical structure).

to be either sub-vertical or sub-horizontal, with no apparent evidence of a temporal sequence between these two orientations. Under crossed-polarized light, V3 veins are characterized by a banding parallel to vein edges (banded veins, Figure 11). Individual vein bands are micrometric with a thickness of ~1 μm on average, similar to that found in banded veins elsewhere [*Renard et al.*, 2005], while the whole vein thickness can range from several μm to several mm.

[21] V3 banded veins are similar to those observed and fully characterized in serpentinites from other geological settings [*Andreani et al.*, 2004; *Renard et al.*, 2005]. Each band corresponds to the discrete infill of a micrometric interstice and is composed of a protoserpentine+ chrysotile+polygonal serpentine assemblage, displaying an overall preferred orientation perpendicular to the local vein wall [*Andreani et al.*, 2004]. Chrysotile and polygonal serpentine grow at the expense of the protoserpen-
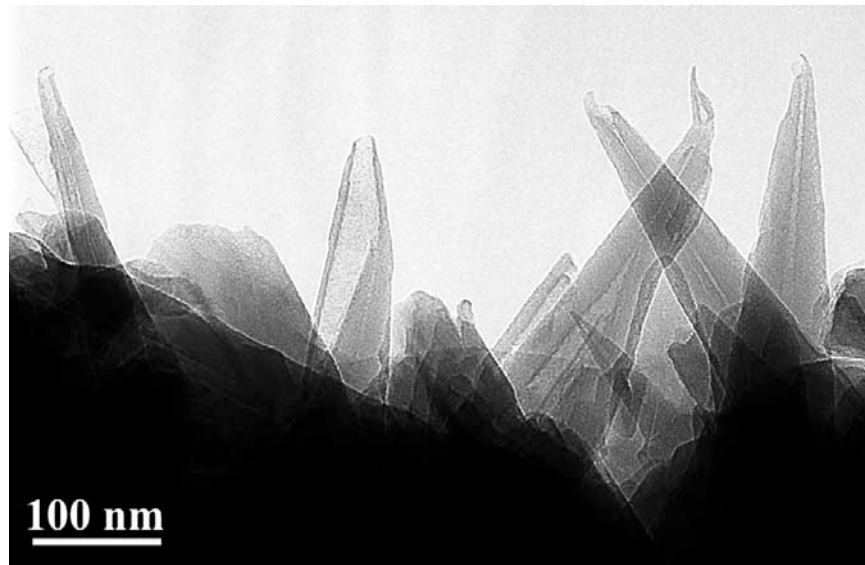
Figure 8. TEM image of conical serpentine tubes that dominantly fill a V1-type vein.

tine, as observed in the V1 veins. Banded veins of this type are inferred to form by repeated crack-seal mechanisms along the same vein [*Ramsay*, 1980].

5.2.4. V4 Vein Type

[22] The last vein generation, V4, is clearly distinguished from the others by non-matching, smooth, irregular walls and a non-fibrous, white aspect of the infill in hand specimen (Figure 5b). Their width is highly irregular, ranging between tens of μm to tens of mm. The distribution of V4 veins appears to be less regular throughout the core than that of the other vein types. They are either observed as isolated veins locally cutting the core or as a well developed network as in Figure 5b. Their length cannot be measured, as they always cut the whole core section, but is at least several cm. V4 veins tend to be perpendicular to the main fabric defined by V2, i.e., sub-vertical on average, except for some core sections where they follow V3 veins, overprinting their banded texture (Figure 11b). Matrix fragments are locally trapped within the vein by crystallization sealing. V4 veins can be intimately associated with Mg-rich carbonates and sulfide grains as illustrated in Figure 12b. These carbonates are likely to represent late stage alteration that may also be responsible for the mono-
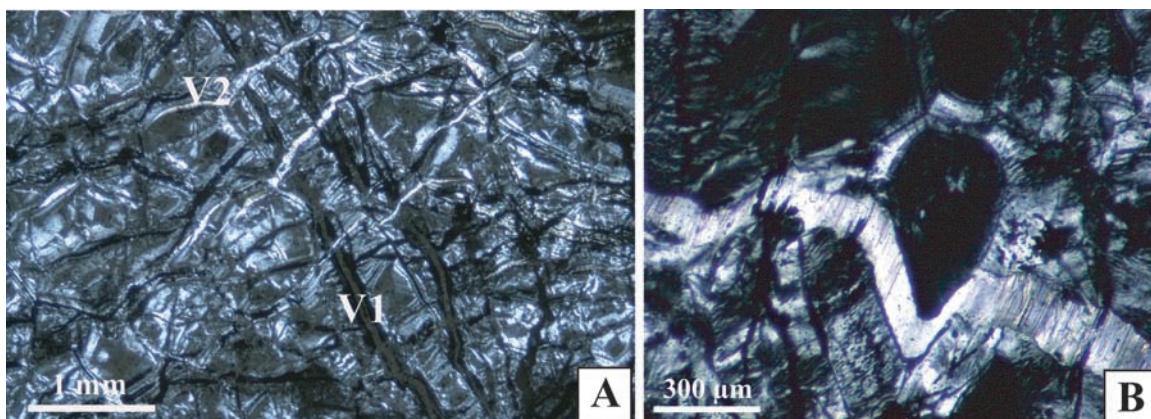

Figure 9. (a) Fibrous serpentine veins of the V2 generation mark an oblique macroscopic fabric (crossed-polarized light image) and cross-cut V1 veins. (b) At the microscopic scale, they tend to follow locally the shape of preexisting olivine grains. Fibers are strictly parallel to each other and indicate an extension perpendicular to the average orientation of the vein (mode I crack).
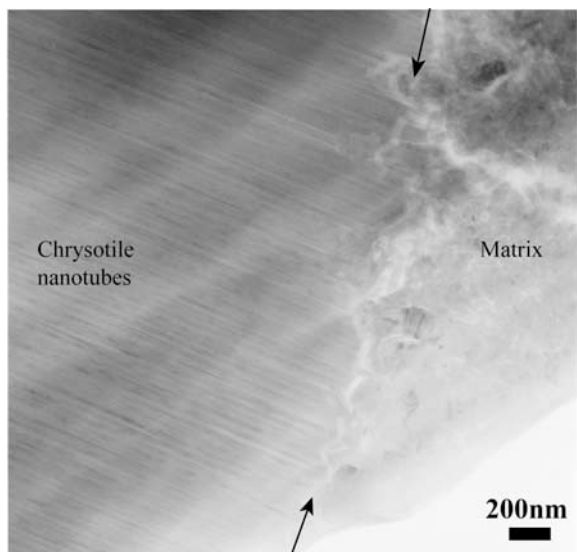
Figure 10. TEM image of the interface between a V2-type vein (homogeneous texture on the left) and the matrix (granular texture on the right). Long parallel nanotubes of chrysotile that fill the V2-type vein are oriented NW-SE on this picture and follow the small-scale veins wall irregularities. The contact between vein and matrix is marked by the arrows.

mineralic aragonite veins found throughout this core.

[23] V4 veins display three different internal textures, alone or together within an individual vein: (1) a symmetric, granular texture formed by micrometric lamellae of serpentine elongated toward the center of the vein (V4a: Figure 12a); (2) a granular texture formed by micrometric spherical serpentine grains as indicated by the black cross extinction under crossed-polarized light (V4b: Figure 12b); and (3) an almost isotropic texture often associated with the previous ones (V4c: Figure 12c) that display similar extinction features with a smaller black cross identified under higher magnification (image at the bottom left of Figure 12c). The lack of clear crosscutting relationships prevents us from establishing a chronological succession for the V4a, b and c vein types.

[24] TEM observations confirm that V4b and V4c microstructural facies have a similar filling texture, the only difference being the grain size (>1 μm for V4b and <1 μm for V4c). This common filling texture is clearly distinct from that of V4a (Figure 13). Figure 13a illustrates the characteristic elongated morphology of triangular serpentine sectors observed in V4a, identified as lizardite. Lizardite elongation is parallel to the c stacking axis, with

the triangular base preferentially oriented toward the center of the vein, as indicated by the optical micrograph in Figure 12a. Lizardite sectors display a high variability in grain size (few tens of nm to several μm) and a mean preferred orientation perpendicular to vein walls (Figure 14). Figure 13b presents the characteristic texture of vein facies V4b and c under the TEM. Elongated sectors of lizardite form a compact texture among which circular shapes are identified. Triangular lizardite sectors seem to grow radially in circular shapes, but as their c-axes are not coplanar, adjacent sectors have different crystallographic orientations that show up as differences in contrast on TEM imagery. We interpret this TEM image as random sections of polyhedral serpentine grains, which are spherical grains with triangular facets [*Andreani*, 2003], as illustrated in Figure 14. Each polyhedral serpentine grain is composed of lizardite sectors joined continuously at their edges
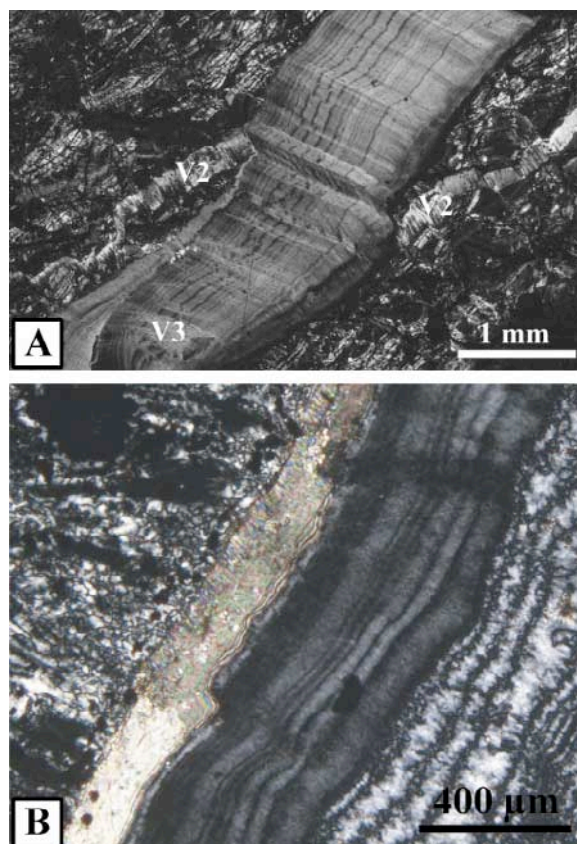

Figure 11. (a) Banded serpentine vein (or "crack-seal type" vein) of the V3 generation that cut a fibrous vein (V2). (b) V3 type vein recrystallized on the right side where it displays a texture similar to V4 vein type. Late carbonate precipitation is observed on the left side of the vein.
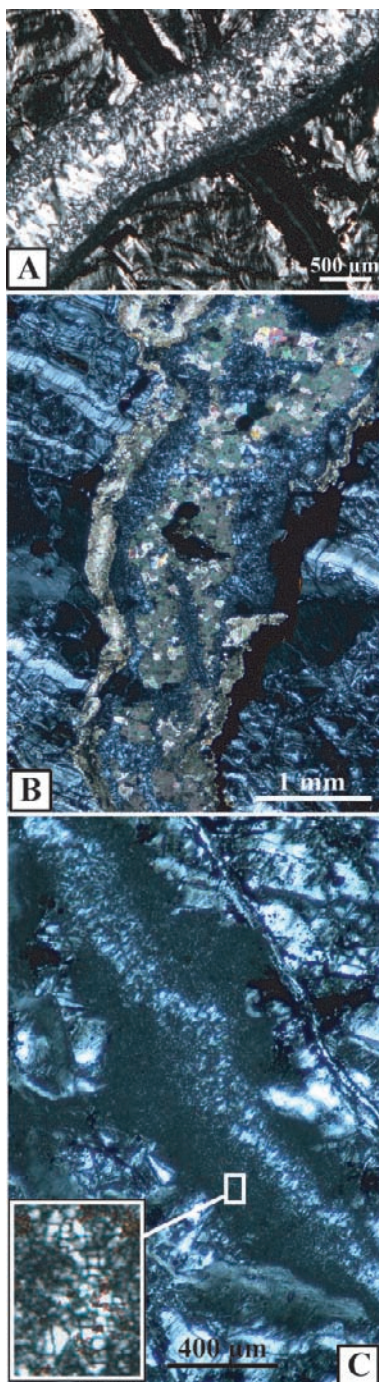
Figure 12. Serpentine veins of the V4 generation. They can be separated into three different categories on the basis of textural criteria: (a) V4a type showing a lamellar texture, (b) V4b type characterized by spherical serpentine grains as evidenced by the black cross extinction under cross-polarized light (associated here with carbonates and sulfides on the right), and (c) V4c type, the intermediate type that can show both a granular texture typical of V4a (vein center) and an almost isotropic texture corresponding to tiny spherical grains (see corner picture) similar to V4b filling material (vein margins).

[*Baronnet et al.*, 2007]. Locally, the poorly crystallized protoserpentine, already identified in V1 and V3, is observed in close contact with the polyhedral serpentine in V4b and V4c veins.

[25] The variability of serpentine microstructures in veins under electron microscopes reflects their textural variability under the optical microscope. This variability suggests different mechanisms of vein formation that should follow different stages of fluid/rock interaction in peridotites. Vein chemistry is required to correlate vein formation mechanisms with the chemical evolution of the system.

6. Vein Chemistry

[26] The formation of serpentine minerals in veins requires the transfer of matter either from the adjacent wall rock by diffusion or dissolution processes, or through the circulation of fluids. In both cases, the formation of the veins is linked with different stages of the serpentinization history affecting the host peridotites. Serpentine minerals are essentially magnesian, but may contain appreciable amounts of Fe, Al, Cr, Ni and other trace elements depending on the chemical composition of their growing environment (see reviews by *O'Hanley* [1996] and *Mével* [2003]). Information about element mobility during serpentinization relative to the timing of hydration events may be inferred from comparison between the composition of relict minerals, serpentine in wall rocks and vein fillings. Analysis of relict minerals and serpentine pseudomorphs and vein fillings are available in appendix (Tables S1, S2, and S3, respectively).

[27] Pseudomorphic serpentine minerals tend to retain the chemical signature of their precursor: Ni in mesh after olivine, and Cr and Al in bastites after pyroxenes. Meshes and bastites show a similar variability in FeO content ranging from 1 to 4 wt%. Meshes are relatively poor in Al ($Al_2O_3 <$ 1 wt%) compared to bastites because the latter retain a part of their initial Al (Al_2O_3 = 1 to 3 wt%). We observe no clear chemical differences between the cores and rims of mesh texture both within partly (50%) and fully (100%) serpentinized rocks, and we therefore group these analyses and serpentinization event under the "mesh" term.

[28] An Al_2O_3 versus FeO diagram (Figure 15) shows that the compositions of the first three generations of veins are similar to that of the mesh. V4b veins are clearly distinct and have a higher Al content that extends from the upper limit of the
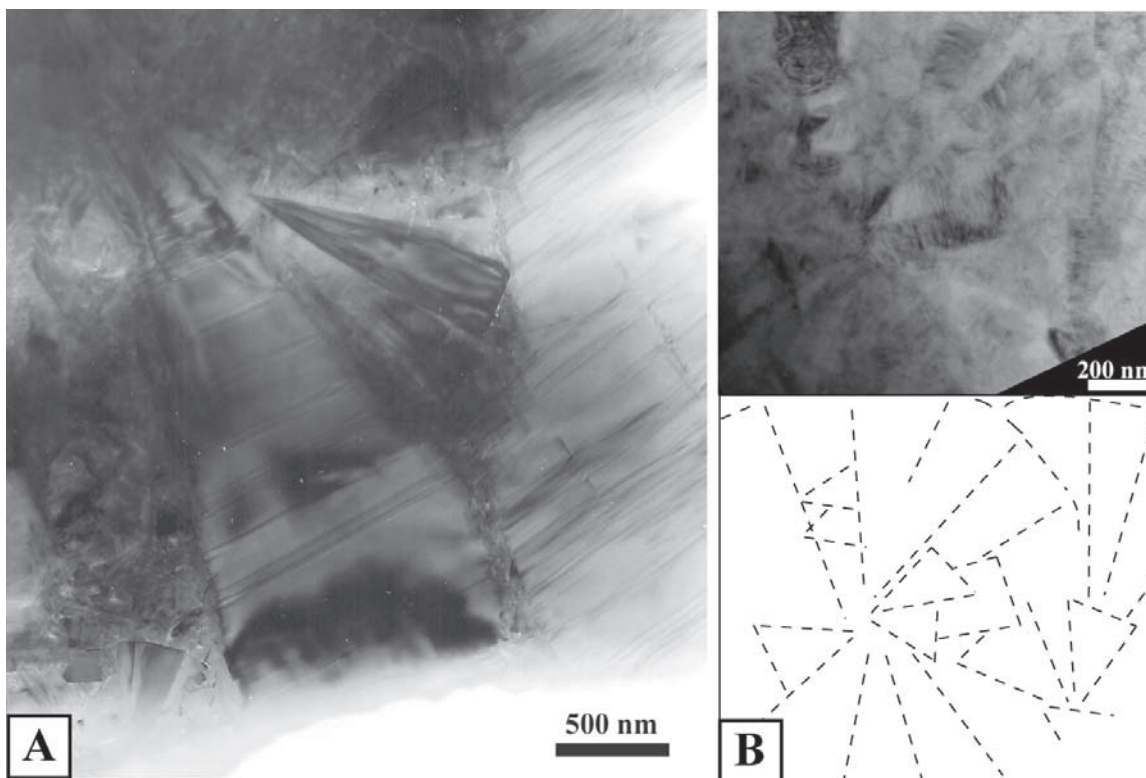
Figure 13. TEM images of lizardite sectors that dominantly fill V4 vein type. In section, lizardite classically displays a triangular morphology with an elongation along the c stacking axis of the sheet structure. Two types of nano-textures can be observed: (a) in V4a veins, the lamellae grow independent of each other and with a mean preferred orientation; (b) in V4b veins, lamellae display variable orientation and are well interlocked. Circular textures suggest radial growth (depicted by dotted lines) and are interpreted in three dimensions as cross sections of spherical morphologies (see Figure 14).

other serpentine veins and mesh (restricted under 1 wt% in Al_2O_3) to values close to those of fresh pyroxenes and bastite (up to 4.3 wt% in Al_2O_3); V4a being intermediate in composition. V4 veins display a less variable FeO content. V3 veins are occasionally recrystallized and display textures (Figure 11b) and compositions similar to V4 (light blue asterisks in Figure 15).

[29] The temporal evolution of chemistry of the local fluid from which the serpentine crystallized in the different veins can be followed by vein chronology and is indicated by the black arrow on Figure 15. Two distinct stages of vein formation are identified on this figure: (1) a first stage with Al-poor fluids in which serpentine of V1 to V3 veins crystallized and (2) a second stage during which fluids richer in Al accompany the formation of serpentines in V4 vein generations.

[30] All serpentine analyses, except those of V4 veins, also contain significant amounts of sulfur, probably located in sulfide micrograins disseminated both in serpentine and among magnetite
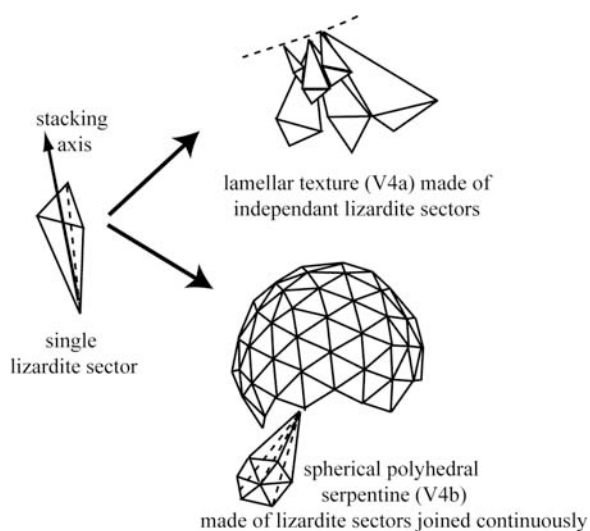

Figure 14. Interpretative schemes in three dimensions of the planar TEM images of Figure 13. V4a are made of independent sectors of lizardite with their growth oriented toward the center of the vein. V4b are made of numerous grains of spherical polyhedral serpentine (faceted serpentine type).
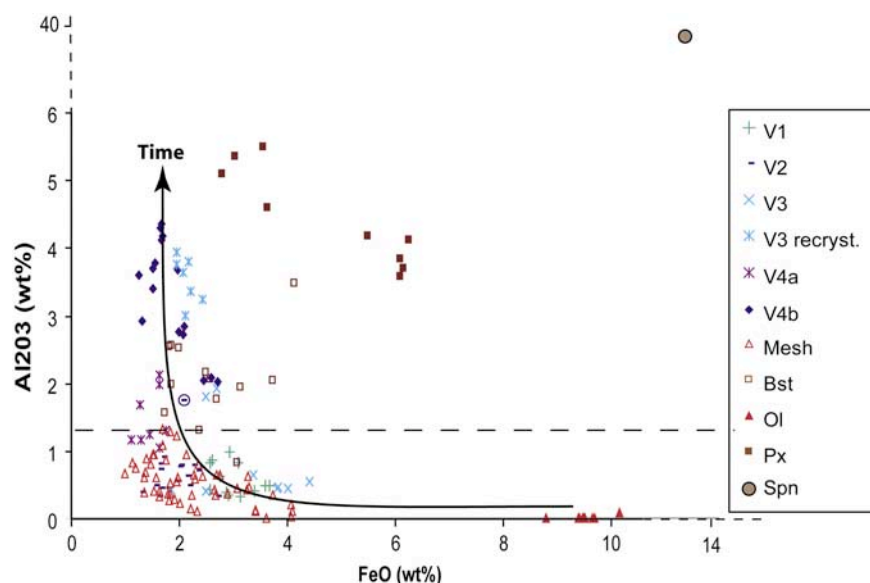
Figure 15. Comparison of the Al_2O_3 and FeO content of the different serpentine veins (V1 to V4) and some representatives compositions of relict minerals (Ol, olivine; Px, pyroxene; Spn, spinel) and pseudomorphic textures (Mesh; Bst, Bastite). The chemical evolution of the system with time (black arrow) is proposed on the basis of vein chronology.

grains in veins [*Gaggero et al.*, 1997; *Alt and Shanks*, 2003]. The high sulfur content of MARK serpentinites has already been noted by *Alt and Shanks* [2003], which they explain by invoking an earlier phase of fluid circulation through grabbros before percolating through ultramafic units.

7. Discussion

7.1. Serpentine Crystallization During Vein Formation

[31] The formation of a vein requires three successive stages: (1) a space opening at a rate that is linked to the stress/strain regime; (2) a transfer of elements to the vein in the presence of a fluid; and (3) a vein-filling episode of mineral crystallization. The kinetics of vein infill will be controlled by the slowest of the mechanical (opening of the vein, fluid advection) or chemical (dissolution, diffusion, precipitation) processes involved, whose kinetics will be constrained contemporaneously by local conditions. Vein-wall morphology provides information on whether the opening mechanism is purely mechanical, chemical (dissolution), or a combination of both. The vein internal structure (crystal orientation and morphology) and chemistry provide information on crystallization mechanism and on the relative rates of opening and sealing. A departure from equilibrium conditions within the

vein is required to initiate crystallization (nucleation and growth). A high degree of disequilibrium will favor kinetic effects on crystallization and can produce first intermediate metastable phases that may eventually evolve to more stable phases during a progressive return to equilibrium conditions. In the case of an aqueous solution, the driving force corresponds to a difference in concentration between the saturated solution at equilibrium and the supersaturated solution in which crystallization can occur. So, crystallization requires a decrease of the equilibrium solubility by changing conditions (P, T, surface energy), an increase of solution concentration by mass transfer, or both. Serpentine microstructures and the chemistry of veins are used here to constrain the different stages of vein formation and the relationship between the physical and chemical conditions at these stages of the exhumation and hydration history of peridotites.

[32] The first stage of veining (V1) is characterized by an iron-rich fluid, as suggested by the abundance of iron oxides along these veins. Iron oxide formation is classically observed within the mesh-textured serpentinites and is mainly associated with the hydration of olivine to form serpentine as in reaction (1). In mesh rims, lizardite mimics olivine outlines in all space directions, suggesting that the alteration process involved very low water/rock ratios [e.g., *Viti and Mellini*, 1998; *Baronnet and*

Boudier, 2001]. Oxide lineations tend to follow the outline of former olivine grains and probably map the early fluid penetration. In contrast, V1 oxides line up along both sides of the diffuse vein walls. This indicates that an aperture, with a minimum width equal to the vein width, was created to initiate V1 formation. Thus a rapid fluid penetration and circulation is enabled within this interconnected network. Contemporaneously, reaction with the nearby hosting matrix can provide the elements for vein infill. Fe-oxide abundance suggests that V1 veins are coeval with the first static hydration of peridotite when primary minerals were dominant in the rocks. This early phase of veining represents an initial opening of a crack network by brittle deformation. Cracks may also extend in length by dissolution processes at the tip. Crystallization of a poorly crystallized material and its subsequent evolution to conical chrysotiles, homogeneously distributed within the vein, requires a rapid crystallization within an open space under high departure from equilibrium in order to favor kinetic effects (see Figure 2). An efficient element supply from the surrounding matrix is necessary, and in situ conditions should favor a rapid dissolution of the matrix, especially the richest iron phase olivine (xFe $\sim$ 0.2 in average). Conical chrysotiles can evolve locally to longer cylindrical chrysotile and polygonal serpentine as conditions return to equilibrium during the crack sealing, but this will be rapidly limited by element arrival. Indeed, the main consequence of this vein formation process is the rapid sealing of cracks, which limits fluid entrance at this stage and stops the hydration reactions.

[33] The purely fibrous texture of the second phase of veining (V2), characterized by the homogeneous diameter and the continuity of cylindrical chrysotile fibers, suggests a single episode of nucleation followed by a continuous growth in length occurring under a constant supersaturation. These microstructures require a constant vein opening velocity, equal or slower than the processes responsible for both the supply of vein infill material and fiber growth [*Hilgers et al.*, 2000; *Koehn et al.*, 2000], so as to avoid the opening of free space that would favor a new nucleation step. The orientation of V2 veins parallel to the detachment fault is probably caused by unroofing tectonics resulting in an extensional stress perpendicular to the free surface. Experiments of *Bons and Jessell* [1997] suggest that fibrous veins may form without fracturing by dissolution-precipitation creep, and that they do not represent major fluid pathways. The mass transfer

to such veins must occur by diffusional transfer, in agreement with the fact that V2 veins are isolated and lens-shaped. Moreover, the slightly higher Al content of the fibers growing in pyroxene cleavages (Al_2O_3 = 1,7 wt%, FeO = 2.1 wt%; Figure 15) compared to those within mesh demonstrate that the source of the vein infill is very local, probably at scales of a few millimeters or less. The presence of associated iron oxides along or within the vein suggests a contemporaneous formation during an episode of Fe-release in the pore fluid. We thus suggest that V2 veins occur immediately after the V1 episode and during the same episode of alteration in which the destabilization of primary minerals releases the iron and the other elements necessary for serpentine formation. This interpretation is also supported by the similarity in composition between the mesh-textured serpentinites and the V1 and V2 vein episodes.

[34] In contrast to V2 veins, the banding observed in V3 veins indicates a series of discrete incremental openings, instead of a continuous one. Each micro-interstice opening is marked by a new nucleation stage of a poorly crystallized phase [*Andreani et al.*, 2004], similar to the one observed in V1 veins. Vein opening velocity is thus faster than serpentine crystallization. As V3 veins do not necessarily form an interconnected network, advection is not possible, and a local mass transfer is required, as inferred for V2 vein formation. Although no conical chrysotile was observed, the evolution of protoserpentine into chrysotile and polygonal serpentines indicates the progressive return to equilibrium conditions. Thus, during the V3 veining episode, supersaturation progressively decreases and crystallization occurs as long as space is available to maintain diffusion along a chemical potential gradient. Capillary effects may be able to increase the departure from equilibrium by lowering solubility in the interstice and help crystallization and diffusive mass transfer [*Baronnet and Saül*, 2003; *Andreani et al.*, 2004]. The chemical composition of V3 vein infill (when not recrystallized) is in the same range as mesh, V1 and V2, indicating that they all belong to the same episode, named Stage 1.

[35] The V4 veining episode appears to correspond to a different fluid circulation and alteration regime, named Stage 2, from that responsible for the successive vein episodes V1 through V3. V4 veins form interconnected fluid pathways, and their smooth, irregular and non-matching walls indicate a progression of dissolution from the vein walls
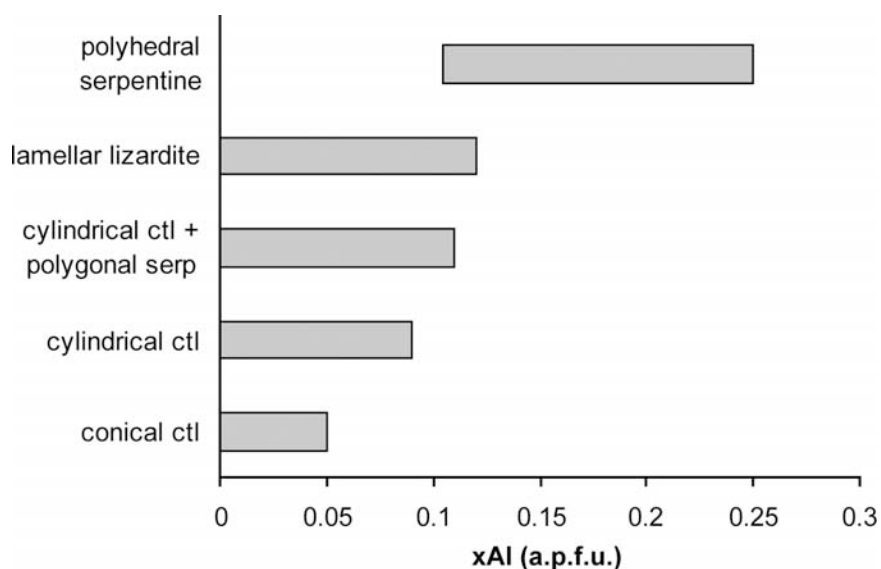
Figure 16. Range of Al content displayed by the main serpentine types observed in veins (a.p.f.u., atom per formula unit; ctl, chrysotile). The role of Al on serpentine microstructure seems predominant for xAl > 0.12

into the matrix. Their internal microstructures require crystallization in an open space were fluids circulate. In the case of V4a veins, the symmetric structure of lizardite grains, enlarging toward the center of the vein, indicates that lizardite nucleated on the vein wall and grew competitively toward the center, with elements provided advectively at the center of the vein. In V4b/c, the more homogeneous distribution of crystals within the veins suggests a higher nucleation rate that is not only localized on vein walls but distributed in the whole vein. Such a texture may have been obtained by progressive recrystallization of a gel-type phase (i.e., the protoserpentine) after its fast and homogeneous precipitation in an open space, in conditions far from equilibrium, like in V1. In contrast to V1, the protoserpentine may have evolved to polyhedral serpentine instead of tubular serpentines (conical and cylindrical chrysotile). The compositional data suggests that Al plays a greater role in the formation of polyhedral serpentine than in the formation of the other types (Figure 16). Polyhedral serpentine occurs at $Al_2O_3 > 2$ wt%, (equivalent to xAl > 0,12). The generally high Al content in the infill of V4 veins ($Al_2O_3 > 1\%$ wt) indicates that their formation occurred in an Al-rich fluid, possibly resulting from the alteration of Al-rich phases, like pyroxenes and spinels, within the partially serpentinized rocks.

[36] V4 formation requires a change in ambient conditions to produce a first stage of serpentine wall dissolution (undersaturated fluid) and a second stage favoring serpentine crystallization in veins (supersaturated fluid). Silicate solubility generally decreases with decreasing P or T conditions. Serpentine crystallization from a fluid thus requires a drop in P or T that may be achieved because of fracture opening. While a pressure drop during fracture opening may favor crystallization, it is inconsistent with the earlier wall dissolution observed, suggesting instead that temperature reduction may be the main controlling factor. Temperature reduction of the fluid can be achieved by its ascension in the upper levels of the cooling lithosphere, probably during late stages of alteration in this area. The local temperature gradient, possibly increased by exothermic serpentinization [*Lowell and Rona*, 2002; *Emmanuel and Berkowitz*, 2006], and the pressure gradient should be able to establish convection cells within the partially serpentinized host rocks and drive fluids toward upper levels. The degree of fluid supersaturation depends on the temperature drop, and it can be reached more or less rapidly depending on fluid velocity.

[37] A summary of microstructural observations and their interpretation in terms of deformation style and mass transfer process along with the veining chronology is proposed in Figure 17. In veins, crystallization kinetics are affected by the deformation rate, which controls the opening rate, the water-to-rock ratio, and mass transfer
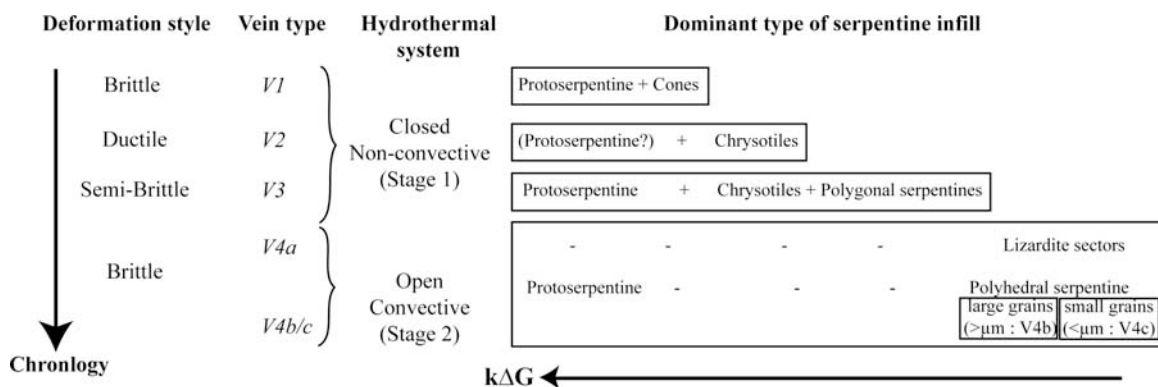
Figure 17. Interpretative summary of the structure and mineralogy of serpentine veins. "kΔG" represents the growth kinetics of the different serpentine according to the studies summarized in Figure 2.

processes. The variety of serpentines observed in MARK veins clearly underlines the role of deformation and of system dynamics on the local departure from equilibrium and consequently on the relative occurrence of serpentine types. It is worth noting that fibrous (curved) structures are preferentially formed during slow deformation rates accommodated by diffusional transfers that favor kinetic effects. This is in accordance with previous studies that suggest chrysotile formation requires higher departure from equilibrium [*Grauby et al.*, 1998, *Normand et al.*, 2002] and is metastable relative to lizardite [*Evans*, 2004].

7.2. Problem of Volume Expansion

[38] Serpentinization of peridotites decreases their density. The average density of a peridotite is 3.3 g/cm³ whereas the average density of a serpentinite is 2.6 g/cm³ [*Deer et al.*, 1966]. On the basis of these average densities, it can be estimated that, under a mass-conservative system, 100% serpentinization results in approximately 27% volume increase. This value actually depends on the modal composition of the peridotite, the composition of the primary minerals, and the initial fluid composition. Alternatively, serpentinization may occur under a volume-conservative system, in which case some elements have to be removed to decrease the rock density. Whether serpentinization occurs at constant mass or constant volume has been largely debated in the literature [e.g., *Thayer*, 1966; *Hostetler et al.*, 1966; *O'Hanley*, 1992]. In highly altered rocks, it is very difficult to reconstruct the mode and composition of the initial peridotite. Moreover, the composition of the reacting fluid phase is essentially unknown. As a consequence, the volume problem is generally

ignored and the serpentinization reactions are written assuming mass conservation. Nevertheless, we must address this question to fully understand serpentinization mechanisms, in particular the coupling between deformation, exhumation and mass transfer.

[39] In the case of the MARK serpentinites, the microstructures in serpentine veins record two main stages of alteration: Stage 1 occurs in a closed-diffusive system with pervasive water arrival and limited convection; Stage 2 occurs in an open system characterized by fluid convection in localized pathways. The absence of grain-scale strain related to volume expansion during olivine and pyroxene replacement by serpentine growth suggests that serpentinization is isovolumic at this scale during both stages. This agrees with previous microstructural observations in the Oman ophiolite [*Baronnet and Boudier*, 2001] and elsewhere [*O'Hanley*, 1992]. Mass transfer is thus necessary to remove excess elements at the olivine/fluid and pyroxene/fluid interfaces. During stage 1, the transfer distance is limited whereas in stage 2, elements may be transported over larger distances and even leave the system.

[40] Stage 1 is characterized by the formation of V1 to V3 veins that generate new volume and may act as a sink for excess elements, as suggested by *O'Hanley* [1992]. Serpentinization may therefore be mass conservative at the scale of the outcrop. Reactions (1) and (2) show that the alteration of olivine and orthopyroxene result in an excess of Mg and Si, respectively, that can be combined to form vein filling serpentine.

[41] Reaction (3) describes the whole system, including the veins, assuming that the volume of the
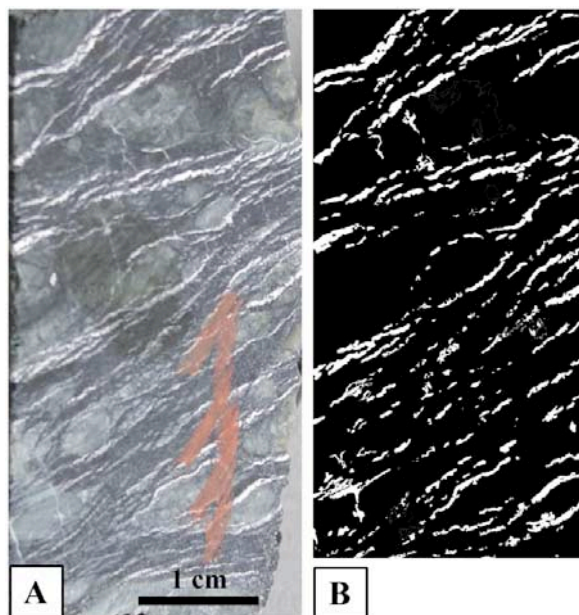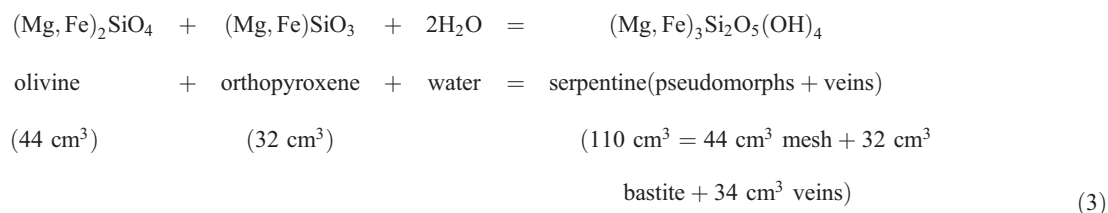
Figure 18. Example of image analysis to estimate the volume of V2 veins. (a) Sample section (153-920B-3R-1, 41–47 cm) displaying a homogeneous vein fabric (V2 vein type). (b) The same section in binary black and white levels that allows an estimation of the surface percentage of veins (in white).

initial minerals (olivine and orthopyroxene) is conserved:

tion at representative lithologies (e.g., sample of Figure 5a). After applying a threshold to separate the veins from the host rock (Figure 18), we estimate that the relative vein volume is at least of 11%. This corresponds to almost 40% serpentinization, according to reaction (3).

[44] V3 veins are likely to accommodate an additional part of the progressing alteration during stage 1. These veins are too scattered in the cores to allow a precise estimation of their volume but, like V1, they do not exceed a few percent. If we consider the V1 to V3 veining events, 40 to 50% of the rock may thus be serpentinized during stage 1 and this serpentinization can be accommodated locally in a closed system, except for the reacting fluid phase. It should be pointed out, however, that these estimates are based on a simplified reaction, in which pseudomorphs after olivine (mesh) have the same compositions as both orthopyroxene pseudomorphs and veins. This is likely not the case. Moreover, neither magnetite, as a product of serpentinization reaction, nor aluminum is not considered. Finally, the composition of the reacting fluid phase is unknown.

[45] To test the applicability of this over-simplified reaction (3), which requires 11% veins for 40% alteration, to the MARK rocks, we can recalculate the vein proportion in a system closer to our

$$
\begin{array}{ccccccc}
(Mg, Fe)_2SiO_4 & + & (Mg, Fe)SiO_3 & + & 2H_2O & = & (Mg, Fe)_3Si_2O_5(OH)_4 \\
\text{olivine} & + & \text{orthopyroxene} & + & \text{water} & = & \text{serpentine(pseudomorphs + veins)} \\
(44\ cm^3) & & (32\ cm^3) & & & & (110\ cm^3 = 44\ cm^3\ \text{mesh} + 32\ cm^3 \\
& & & & & & \text{bastite} + 34\ cm^3\ \text{veins})
\end{array}
\tag{3}
$$

This reaction results in a volume increase of 34 cm^3 for a complete serpentinization, which correspond to ~45% of the initial volume, and ~30% of the final volume.

[42] The maximum volume created by V1 opening by thermal cracking is likely to be restricted. Thin section optical estimates of V1 volume percentage do not exceed 5%. Moreover, this very limited permeability is rapidly sealed by the formation of serpentine in available space.

[43] V2 is the most abundant vein in MARK serpentinites. We can reasonably assume that these veins are planar and estimate their volume from their area observed in perpendicular cutting surfaces. We have selected 3 digital images of areas with well-developed homogeneous vein distribu-

observations. We consider a peridotite composed of 80% of olivine and 20% of orthopyroxene, as in the MARK rocks. We use an average composition for the different mineral phases calculated from microprobe analyses (Tables S1 to S3) and their molar volume (as in reaction (3) [*Deer et al.*, 1966]). We estimate that the best mass balance is obtained when about 1/3 of the initial olivine (i.e., 25 wt% of the initial peridotites) reacts with half of the initial orthopyroxene (i.e., 10 wt% of initial peridotites) (Table S4), producing ~37% of serpentinization for ~12% veins. This rough calculation fits our microstructural observations. The amount of pyroxene involved may be reduced if the hydrating fluid has been enriched in silica by percolated within the mafic unit before entering the peridotite, as suggested by *Alt and Shanks* [2003].

[46] During stage 2, the excess matter can be removed by fluid convection in an open system and serpentinization can be completed. The V4 vein chemistry suggests an Al release which probably corresponds to the late alteration of remaining pyroxene and spinel.

7.3. Temperature of Serpentinization

[47] The similar composition of the V1, V2, V3 veins (except recrystallized ones) and most of the mesh (1 < FeO < 4 wt%; Al < 1wt%; SO_3 > 0,1wt%) suggests a formation under similar conditions and fluid composition. Oxygen isotope studies on the serpentine-magnetite pair (geothermometer of *Wenner and Taylor* [1971]) indicate that the serpentinization by seawater occurred at temperatures from >350–400°C to <200°C [*Hebert et al.*, 1990], but with a very large uncertainty (±100°C) because of the poor calibration of the thermometer [*Agrinier and Cannat*, 1997]. Studies of opaque minerals restrict the first fluid temperature to <400°C [*Alt and Shanks*, 2003] and suggest a fluid reaction with mafic rocks prior to hydration to account for the sulfur content and isotopic composition of MARK serpentinites. At this temperature of ~400°C, the kinetics of orthopyroxene reaction with water is higher than that of olivine (stable for T > 350°C), which should favor pyroxene alteration to talc [*Martin and Fyfe*, 1970; *Bach et al.*, 2004] while generating an increase of Si activity and a release of Al into the fluid. However, talc, tremolite or chlorite are seldom observed in these cores. Pyroxene relicts are more abundant than olivine relicts, and pyroxenes, when altered, are transformed to serpentine. The first stage veins (V1, V2, V3) and mesh indicate that there is some Al in the fluid and that a part of Si should be provided by pyroxene alteration, which may have prevented brucite formation at the beginning of alteration. However, olivine dissolution should control the chemistry to stay in the serpentine domain of formation. This is also suggested by the abundance of magnetite within the mesh and the V1 and V2 veins. Pyroxene reactivity is maximum at T > 400°C, but pyroxene is less reactive at lower T under which olivine dissolution dominates [*Janecky and Seyfried*, 1986], peaking at ~250°C. On the basis of these observations and the previous data, the first stage of serpentinization in the MARK area appears to have occurred at an intermediate temperature T < 300–350°C, initiating at a minimum sub-seafloor depth of ~3–4 km, which is near the seismic Moho according to the interpretation of the seismic velocity profile (Figure 4).

[48] V4 vein sealing occurred after the first 50% of alteration, during the last stage of rock exhumation in shallow lithospheric levels <2 km if we assume that the seismic Moho maps the alteration profile at this site. This correspond to a temperature <150–200°C by using the previous estimation of 350°C at 4 km and the hypothesis of a constant temperature gradient in the crust.

7.4. Water Circulation and Alteration

[49] Hydration of the oceanic lithosphere requires penetration of fluids, but the mechanisms and the depth of fluid penetration and the evolution of serpentinization are poorly understood. Anisotropic thermal contraction of olivine during uplift can result in cracking along grain boundaries and create an interconnected microcrack network enabling fluid penetration [*de Martin et al.*, 2004]. This process would be limited to the shallow crust (~4–6 km, corresponding to the 400°C isotherm) and to the end of mid-ocean ridge segments, provided that the cooling rates are sufficiently high. Additional cracking can be induced by near-axis seismicity, which shows focal depths of up to 8 km near Site 920D (MAR at 23°N [*Toomey et al.*, 1988]) and near other sites along the MAR (e.g., 29°N [*Wolfe et al.*, 1995] and 5°S [*Tilmann et al.*, 2004]). These depths are well below the ~3–4 km transition from a seismic velocity gradient to velocities typical of unaltered mantle found at this site [*Canales et al.*, 2000]. These observations suggest that deformation of the brittle lithosphere enables the deep penetration of water (probably >6 km), but that serpentinization only occurs in the shallow levels of the system (<4 km). The early stages of veining and alteration (V1 and mesh texture initiation), being associated with a low degree of serpentinization (<5%), can thus occur throughout the whole system and at depths well below the 3–4 km "seismic Moho." As such, a low degree of alteration may not be resolved by the existing seismic data [*Miller and Christensen*, 1997]. The stress field and active chemical reactions between aqueous fluid and anhydrous minerals at vein tips can also drive vein propagation deeper than expected by simple brittle cracking [e.g., *Jamtveit et al.*, 2000]. This alteration can be attained at short geological timescales (i.e., at zero-age oceanic lithosphere), as indicated by experimental data on serpentinization of olivine (5% alteration of olivine within a day [*Martin and Fyfe*, 1970] and by the formation of conical serpentines in synthesis experiments at similar timescales [*Grauby et al.*, 1998]). Rapid hydration should also seal the
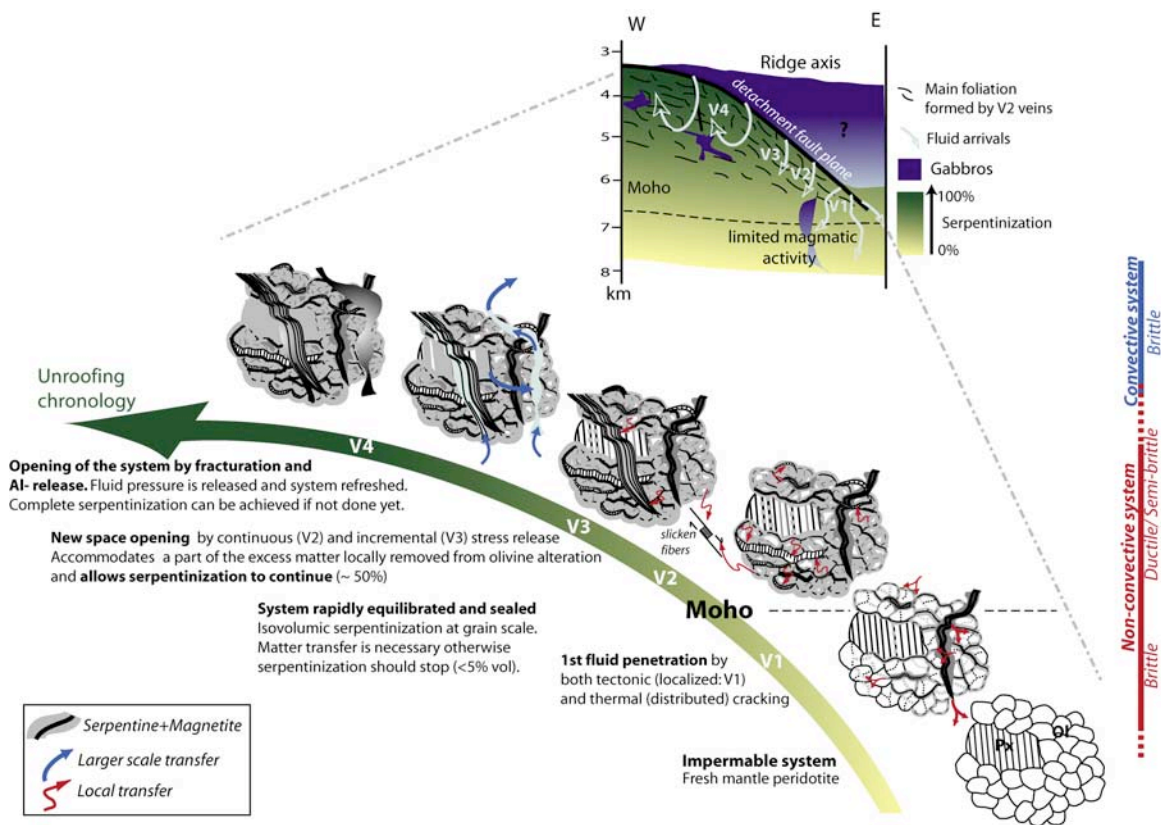
Figure 19. Proposed model of serpentine vein formation and hydrothermal circulation during the progressive unroofing of peridotites exposed in the MARK area.

available permeability and prevent further alteration once the available water is consumed.

[50] The later vein stages V2 and V3 renewed crack formation that accommodate the volume expansion during hydration of primary minerals and enable serpentinization to continue and reach ∼40%. These reactions occur in a closed system with the only addition of water that should pervasively penetrate the massive rock in the absence of fluid pathways at this stage. Numerical models of hydrothermal circulation and serpentinization by *Emmanuel and Berkowitz* [2006] indicate that, in a saturated system with sufficient permeability, hydration can induce downward flow and consume available water, preventing hydrothermal convection [see *Emmanuel and Berkowitz*, 2006, Figure 6a]. V1 veins are associated with a low degree of alteration (∼5%) that may correspond to this mode of alteration in the numerical models. Alteration can progress in the absence of substantial hydrothermal circulation (convection cells) either in early stages of the model cycle (<2000 years) or in portions of the system isolated from the main circulation cells at later stages [see *Emmanuel*

and Berkowitz, 2006, Figure 4]. These areas of reduced fluid circulation can enable up to 50% serpentinization, consistent with the characteristics of the V2–V3 veining episodes, and operating primarily between the seismic Moho (∼4 km) and ∼2 km (interpretation of Figure 4). The latest veining episode (V4) is restricted to the upper ∼2 km of the lithosphere, corresponding to degrees of serpentinization >50% (seismic velocity profile), where an open system of hydrothermal circulation operates.

[51] The homogeneous fiber orientation in V2 veins throughout the core indicates a homogeneous anisotropic extension in the MARK area during this stage resulting from a progressive unroofing along a major fault. The transition from the regular distribution of V2 veins in the cores to more localized V3 veins and highly localized V4 veins may record the ductile to brittle transition in serpentinites at a depth of ∼2 km. These observations underline the control of unroofing tectonics, coupled with the evolution of the deformation regime, on hydration processes and fluid circulation.

[52] The complex history of alteration of the oceanic lithosphere based on the MARK observations is summarized in Figure 19.

8. Conclusions

[53] 1. We have identified four veining phases associated with the overall serpentinization of the oceanic lithosphere at the MARK site. Serpentine microstructures and the composition of these veins provide information on the relative rates of crack opening and vein mineral precipitation, on the crystallization conditions, and on the temporal evolution of alteration.

[54] 2. The first three vein phases (V1−V3) are associated with the formation of 40% to 50% of the serpentinization by accommodating the volume expansion required within a closed system, where local mass transfer and diffusion processes dominate. The last vein episode (V4) records instead an open system of hydrothermal circulation that enables transport of excess elements from hydration reactions and permits full serpentinization.

[55] 3. Rough depth constraints on the occurrence of these vein episodes are given by comparison with seismic velocity data in the area. The initial phase of serpentinization occurred at 300−350°C. V1 veins may have formed early at depths of up to 8 km, corresponding to the maximum depth of axial seismicity in the area and elsewhere. As they are associated with very low degrees of alteration (<5%), their presence cannot be constrained by seismic refraction data and may be present in seismically "unaltered" mantle (i.e., below the ∼4 km seismic Moho). V2 and V3 veins, associated with a hydration of up to ∼50% of the mantle rocks, can form between the ∼4 km deep Moho and ∼2 km. The transition to an open system recorded by the V4 veins, with higher fluid/rock ratios and completion of serpentinization of the lithosphere, is probably restricted to shallow lithospheric levels (<∼2 km) where major fracturing and advective mass transport dominate.

[56] 4. Not all veins are always open fluid pathways or late episodes of alteration. Instead they can record local diffusive mass transfer and accompany the serpentinization process from very early in the hydration history of the lithosphere. The capacity of some veins to accommodate the volume increase required for serpentinization also highlights the major control of local tectonics on hydration processes by cooling and faulting and may differ from one site to another. Full serpentinization thus requires creation of porosity through extensional tectonics and unroofing that probably control the transition from an early closed, non-convective hydrothermal system to an open, convective hydrothermal system. Important feedbacks are expected between the hydrodynamic properties of the system (permeability, porosity) and physico-chemical processes (dissolution, diffusion, crystallization). Further identification and quantification of these processes are required to fully understand the evolution of the alteration of the oceanic lithosphere and the associated changes in chemical and physical properties.

Acknowledgments

References

Agrinier, P., and M. Cannat (1997), Oxygen-isotope constraints on serpentinization processes in ultramafic rocks from the Mid-Atlantic Ridge (23°N), *Proc. Ocean Drill. Program Sci. Results*, *153*, 381−388.

Allen, D. E., and W. E. Seyfried (2003), Compositional controls on vent fluids from ultramafic-hosted hydrothermal systems at mid-ocean ridges: An experimental study at 400°C, 500 bars, *Geochim. Cosmochim. Acta*, *67*, 1531−1542.

Allen, D. E., and W. E. Seyfried (2004), Serpentinization and heat generation: Constraints from Lost City and Rainbow hydrothermal systems *Geochim. Cosmochim. Acta*, *68*, 1347−1354.

Alt, C. J., and W. C. Shanks (2003), Serpentinization of abyssal peridotites from the MARK area, Mid-Atlantic Ridge: Sulphur geochemistry and reaction modelling, *Geochim. Cosmochim. Acta*, *67*, 641−653.

Andreani, M. (2003), Les microstructures de déformation des serpentines et la partition sismique-asismique: Exemple de la Californie, Ph.D. thesis, Univ. Joseph Fourier, Grenoble1, Grenoble, France.

Andreani, M., A. Baronnet, A.-M. Boullier, and J.-P. Gratier (2004), A microstructural study of a crack-seal type serpentine vein, using SEM and TEM techniques, *Eur. J. Mineral.*, *16*, 585−595.

Bach, W., C. J. Garrido, H. Paulick, J. Harvey, and M. Rosner (2004), Seawater-peridotite interactions: First insights from ODP Leg 209. MAR 15°N, *Geochem. Geophys. Geosyst.*, *5*, Q09F26, doi:10.1029/2004GC000744.

Baronnet, A., and F. Boudier (2001), Microstructural and microchemical aspect of serpentinization, in *Eleventh V. M. Goldschmidt Conference*, Abstract 3382, Lunar and Planet. Inst., Houston, Tex.

Baronnet, A.. and A. Saül (2003), Interstitial crystal growth from undersaturated solutions: A model and geological applications, in paper presented at EGS-AGU-EUG Joint Assembly, Eur. Geophys. Soc., Nice, France.

Baronnet, A., M. Andreani, O. Grauby, B. Devouard, S. Nitsche, and D. Chaudanson (2007), Onion morphology and microstructure of polyhedral serpentine, *Am. Mineral*, in press.

Bons, P. D., and M. W. Jessell (1997), Experimental simulation of the formation of fibrous veins by localised dissolution-precipitation creep, *Mineral. Mag.*, 61, 53–63.

Brown, J. R., and J. A. Karson (1988), Variations in axial processes on the Mid-Atlantic Ridge: The median valley of the MARK area, *Mar. Geophys. Res.*, 10, 109–138.

Canales, J. P., J. A. Collins, J. Escartin, and R. S. Detrick (2000), Seismic structure across the rift valley of the Mid-Atlantic ridge at 23°20′N (MARK area): Implications for crustal accretion processes at slow-spreading ridges, *J. Geophys. Res.*, 105, 28,411–28,425.

Cann, J. R., D. K. Blackman, D. K. Smith, E. McAllister, B. Janssen, S. Mello, E. Avgerinos, A. R. Pascoe, and J. Escartín (1997), Corrugated slip surfaces formed at North Atlantic ridge-transform intersections, *Nature*, 385, 329–332.

Cannat, M. (1993), Emplacement of mantle rocks in the seafloor at mid-ocean ridges, *J. Geophys. Res.*, 98, 4163–4172.

Cannat, M., et al. (1995a), Thin crust, ultramafic exposures, and rugged faulting patterns at Mid-Atlantic Ridge (22°–24°N), *Geology*, 23, 49–52.

Cannat, M., J. A. Karson, D. J. Miller. and the Shipboard Scientific Party of ODP Leg 153 (1995b), *Proceedings of the Ocean Drilling Program, Initial Reports*, vol. 153, Ocean Drill. Program, College Station, Tex.

Carlson, R. L., and D. J. Miller (1997), A new assessment of the abundance of serpentinite in the oceanic crust, *Geophys. Res. Lett.*, 24, 457–460.

Caruso, L. J., and J. V. Chernosky (1979), The stability of lizardite, *Can. Mineral.*, 17, 757–769.

Ceuleneer, G., and M. Cannat (1997), High-temperature ductile deformation of site 920 peridotites, *Proc. Ocean Drill. Program Sci. Results*, 153, 35–59.

Charlou, J.-L., Y. Fouquet, H. Bougault, J-.P. Donval, J. Etoubleau, A. Jean-Baptiste, P. Appriou, and P. A. Rona (1998), Intense CH_4 plume generated by serpentinization of ultramafic rocks at the intersection of the 15°20′N fracture zone and the Mid-Atlantic Ridge, *Geochim. Cosmochim. Acta*, 62, 2323–2333.

Chernosky, J. V. J. (1973), An experimental investigation of the serpentine and chlorite group minerals in the system $MgO-Al2O_3-SiO_2-H_2O$, Ph.D. thesis, Mass. Inst. of Technol., Cambridge.

Chernosky, J. V., R. G. Berman, and L. T. Bryndzia (1988), Stability, phase relations, and the thermodynamic properties of chlorite and serpentine group minerals, in *Hydrous Phyllosilicates*, *Rev. Mineral.*, vol. 19, edited by S. W. Bailey, pp. 295–346, Mineral. Soc. of Am., Washington, D. C.

Christensen, N. I. (1972), The abundance of serpentinites in the oceanic crust, *J. Geol.*, 80, 709–719.

de Martin, B., G. Hirth, and B. Evans (2004), Experimental constraints on thermal cracking of peridotites at ocean spreading centers, in *Mid-Ocean Ridges: Hydrothermal Interactions Between the Lithosphere and Oceans*, *Geophys. Monogr. Ser.*, vol. 148, edited by C. R. German, J. Lin, and L. M. Parson, pp. 167–185, AGU, Washington, D. C.

Deer, W. A., R. A. Howie, and J. Zussman (1966), *An Introduction to the Rock-Forming Minerals*, 528 pp., Longman, New York.

Devouard, B., A. Baronnet, G. Van Tendeloo, and S. Amelinckx (1997), First evidence of synthetic polygonal serpentines, *Eur. J. Mineral.*, 9, 539–546.

Dick, H. J. B. (1989), Abyssal peridotites, very slow spreading ridges and ocean ridge magmatism, in *Magmatism in the Ocean Basins*, edited by A. D. Saunders. and M. J. Norry, *Geol. Soc. Spec. Publ.*, 42, 71-105.

Dilek, Y., A. J. Coulton, and S. D. Hurst (1997), Serpentinization and hydrothermal veining in peridotites at site 920 in the Mark area, *Proc. Ocean Drill. Program Sci. Results*, 153, 35–59.

Dungan, M. A. (1979), A microprobe study of antigorite and some serpentine polymorphs, *Can. Mineral.*, 17, 771–784.

Dyment, J., J. Arkani-Hamed, and A. Ghods (1997), Contribution of serpentinized ultramafics to marine magnetic anomalies at slow and intermediate spreading centers: Insights from the shape of the anomalies, *Geophys. J. Inter.*, 129, 691–701.

Emmanuel, S., and B. Berkowitz (2006), Suppression and stimulation of seafloor hydrothermal convection by exothermic mineral hydration, *Earth Planet. Sci. Lett.*, 243, 657–668.

Escartín, J., G. Hirth, and B. Evans (1997), Effects of serpentinization on the lithospheric strength and the style of normal faulting at slow-spreading ridges, *Earth Planet. Sci. Lett.*, 151, 181–190.

Escartín, J., G. Hirth, and B. Evans (2001), Strength of slightly serpentinized peridotites: Implications for the tectonics of oceanic lithosphere, *Geology*, 29, 1023–1026.

Evans, B. W. (2004), The serpentinite multisystem revisited: Chrysotile is metastable, *Int. Geol. Rev.*, 46, 479–506.

Evans, B. W., W. Johannes, H. Oterdoom, and V. Trommsdorf (1976), Stability of chrysotile and antigorite in the serpentine multisystem, *Schweiz. Mineral. Petrogr. Mitt.*, 56, 79–93.

Früh-Green, G. L., A. Plas, and C. Lécuyer (1996), Petrologic and stable isotopes constraints on hydrothermal alteration and serpentinization of the EPR shallow mantle at Hess-Deep (site 895), *Proc. Ocean Drill. Program Sci. Results*, 147, 255–287.

Gaggero, L., L. Cortesogno, and M. Gazzotti (1997), Data report: Oxides, sulfides, and associated phases in veins and hydrothermally altered peridotitic rocks, *Proc. Ocean Drill. Program Sci. Results*, 153, 523–530.

Grauby, O., A. Baronnet, B. Devouard, K. Schoumacker, and L. Demirdjian (1998), The chrysotile-polygonal serpentine-lizardite suite synthesized from a $3MgO-2SiO_2-excess H_2O$ gel, in *The 7th International Symposium on Experimental Mineralogy, Petrology, and Geochemistry*, *Terra Nova*, 10, suppl., 24.

Grobety, B., A. Plas, and G. L. Früh-Green (1997), Serpentinization temperature of ocean floor peridotites from the Hess Deep rift valley, Pacific Ocean, *Terra Nova*, 9, 549.

Hebert, R., A. C. Adamson, and S. C. Komor (1990), Metamorphic petrology of ODP leg 109, Hole 670A serpentinized peridotites: Serpentinization processes at slow spreading ridge environment, *Proc. Ocean Drill. Program Sci. Results*, 106/109, 103–115.

Hilgers, C., D. Köhn, P. D. Bons, and J. L. Urai (2000), Development of crystal morphology during unitaxial growth in a progressive widening vein: II. Numerical simulations of the evolution of antitaxial fibrous veins, *J. Struct. Geol.*, 23, 873–885.

Holm, N. G., and J.-L. Charlou (2001), Initial indications of abiotic formation of hydrocarbons in the Rainbow ultramafic hydrothermal system, *Mid-Atlantic Ridge, Earth Planet. Sci. Lett.*, 191, 1–8.

Hostetler, P. B., R. G. Coleman, F. A. Mumpton, and B. W. Evans (1966), Brucite in alpine serpentinites, *Am. Mineral.*, *51*, 75–98.

Jamtveit, B., H. Austrheim, and A. Malthe-Sorensen (2000), Accelerated hydration of the Earth's deep crust induced by stress perturbations, *Nature*, *408*, 75–78.

Janecky, D. R., and W. E. Seyfried (1986), Hydrothermal serpentinization of peridotite within the oceanic crust: Experimental investigations of mineralogy and major element chemistry, *Geochim. Cosmochim. Acta*, *50*, 1357–1378.

Johannes, W. (1968), Experimental investigation of the reaction forsterite + H_2O = serpentine + brucite, *Contrib. Mineral. Petrol.*, *19*, 309–315.

Karson, J. A., and R. M. Lawrence (1997), Tectonic setting of serpentinites exposure on the western median valley wall of the MARK are in the vicinity of site 920, *Proc. Ocean Drill. Program Sci. Results*, *153*, 5–21.

Karson, J. A., et al. (1987), Along-axis variations in seafloor spreading in the MARK area, *Nature*, *328*, 681–685.

Kelley, D. S., et al. (2001), An off-axis hydrothermal vent field discovered near the Mid-Atlantic Ridge at 30°N, *Nature*, *412*, 145–149.

Koehn, D., C. Hilgers, P. D. Bons, and C. W. Passchier (2000), Numerical simulation of fiber growth in antitaxial strain fringes, *J. Struct. Geol.*, *22*, 1311–1324.

Lagabrielle, Y., D. Bideau, M. Cannat, J. A. Karson. and C. Mével (1998), Ultramafic-mafic plutonic rock suites exposed along the Mid-Atlantic Ridge (10°N–30°N): Symmetrical-asymmetrical distribution and implications for seafloor spreading processes, in *Faulting and Magmatism at Mid-Ocean Ridges*, *Geophys. Monogr. Ser.*, vol. 106, edited by W. R. Buck et al., pp. 153–176, AGU, Washington, D. C.

Lowell, R. P., and P. A. Rona (2002), Seafloor hydrothermal systems driven by the serpentinization of peridotite, *Geophys. Res. Lett.*, *29*(11), 1531, doi:10.1029/2001GL014411.

Martin, B., and W. S. Fyfe (1970), Some experimental and theoretical observations on the kinetics of hydration reactions with particular reference to serpentinization, *Chem. Geol.*, *6*, 185–195.

Mével, C. (2003), Serpentinization of abyssal peridotites at mid-ocean ridges, *C.R. Géosci.*, *335*, 825–852.

Mével, C., M. Cannat, P. Gente, E. Marion, J.-M. Auzende, and J. A. Karson (1991), Emplacement of deep crustal and mantle rocks on the west median valley wall of the MARK area (MAR 23°N), *Tectonophysics*, *190*, 31–53.

Miller, D. J., and N. I. Christensen (1997), Seismic velocities of lower crustal and upper mantle rocks from the slow-spreading Mid-Atlantic Ridge, south of the Kane transform fault, *Proc. Ocean Drill. Program Sci. Results*, *153*, 437–454.

Moore, D. E., D. A. Lockner, M. Shengli, R. Summers, and J. D. Byerlee (1997), Strengths of serpentinites gouges at elevated temperatures, *J. Geophys. Res.*, *102*, 14,787–14,801.

Normand, C., A. E. Williams-Jones, R. F. Martin, and H. Vali (2002), Hydrothermal alteration of olivine in a flow-through autoclave: Nucleation and growth of serpentine phases, *Am. Mineral.*, *87*, 1699–1709.

O'Hanley, D. S. (1992), Solution to the volume problem in serpentinization, *Geology*, *20*, 705–708.

O'Hanley, D. S. (1996), *Serpentinites: Records of Tectonic and Petrological History*, Oxford Univ. Press, New York.

O'Hanley, D. S., and F. J. Wicks (1995), Conditions of formations of lizardite, chrysotile and antigorite, Cassiar, British Columbia, *Can. Mineral.*, *33*, 753–773.

Ramsay, J. G. (1980), The crack-seal mechanism of rock deformation, *Nature*, *284*, 135–139.

Renard, F., M. Andreani, A.-M. Boullier, and P. Labaume (2005), Crack-seal patterns: Records of uncorrelated stress release variations in crustal rocks, in *Deformation Mechanisms, Rheology and Tectonics: From Minerals to the Lithosphere*, edited by D. Gapais et al., *Geol. Soc. Spec. Publ.*, *243*, 67–79.

Thayer, T. P. (1966), Serpentinization as a constant-volume metasomatic process, *Am. Mineral.*, *51*, 685–710.

Tilmann, F., E. Flueh, L. Planert, T. Reston, and W. Weinrebe (2004), Microearthquake seismicity of the Mid-Atlantic Ridge at 5°S: A view of tectonic extension, *J. Geophys. Res.*, *109*, B06102, doi:10.1029/2003JB002827.

Toomey, D. R., G. M. Purdy, and S. C. Solomon (1988), Microearthquakes beneath the median valley of the Mid-Atlantic ridge near 23°N: Tomography and tectonics, *J. Geophys. Res.*, *93*, 9093–9112.

Tucholke, B. E., J. Lin, and M. C. Kleinrock (1998), Megamullions and mullion structure defining oceanic metamorphic core complexes on the Mid-Atlantic Ridge, *J. Geophys. Res.*, *103*, 9857–9866.

Viti, C., and M. Mellini (1998), Mesh textures and bastites in the Elba retrograde serpentinites, *Eur. J. Mineral.*, *10*, 1341–1359.

Wenner, D. B., and H. P. Taylor (1971), Temperature of serpentinization of ultramafic rocks based on O^{18}/O^{16} fractionation between coexisting serpentine and magnetite, *Contrib. Mineral. Petrol.*, *32*, 165–185.

Wicks, F. J., and D. S. O'Hanley (1988), Serpentine minerals: Structures and petrology, in *Hydrous Phyllosilicates*, *Rev. Mineral.*, vol. 19, edited by S. Bailey, pp. 91–167, Mineral. Soc. of Am., Washington, D. C.

Wicks, F. J., and E. J. W. Whittaker (1975), A reappraisal of the structures of the serpentine minerals, *Can. Mineral.*, *13*, 227–243.

Wicks, F. J., and E. J. W. Whittaker (1977), Serpentine texture and serpentinization, *Can. Mineral.*, *15*, 459–488.

Wolfe, C., G. M. Purdy, D. R. Toomey, and S. C. Solomon (1995), Microearthquake characteristics and crustal velocity structure at 29°N of the Mid-Atlantic Ridge: The architecture of a slow-spreading segment, *J. Geophys. Res.*, *100*, 24,449–24,472.

Yada, K., and K. Iishi (1974), Serpentine minerals hydrothermally synthesized and their microstructures, *J. Crystal Growth*, *24/25*, 627–630.